PHYSICAL REVIEW D **73,** 114505 (2006)

Electromagnetic and spin polarizabilities in lattice QCD

W. Detmold,[1,*] B. C. Tiburzi,[2,†] and A. Walker-Loud[1,‡]

[1]*Department of Physics, University of Washington, Box 351560, Seattle, Washington 98195-1560, USA*
[2]*Department of Physics, Duke University, P.O. Box 90305, Durham, North Carolina 27708-0305, USA*

(Received 11 April 2006; published 12 June 2006)

We discuss the extraction of the electromagnetic and spin polarizabilities of nucleons from lattice QCD. We show that the external field method can be used to measure all the electromagnetic and spin polarizabilities including those of charged particles. We then turn to the extrapolations required to connect such calculations to experiment in the context of finite volume chiral perturbation theory. We derive results relevant for lattice simulations of QCD, partially-quenched QCD and quenched QCD. Our results for the polarizabilities show a strong dependence on the lattice volume and quark masses, typically differing from the infinite volume limit by $\sim$10% for current lattice volumes and quark masses.

DOI: 10.1103/PhysRevD.73.114505 PACS numbers: 12.38.Gc

I. INTRODUCTION

Compton scattering at low energies is an invaluable tool with which to study the electromagnetic structure of hadrons. At very low photon energies, the Compton amplitude is dominated by pointlike photon scattering from the total charge and magnetic moment of the target hadrons. As the frequency increases, contributions beyond pointlike scattering enter, and one begins to resolve the hadronic response to an applied electromagnetic field. For unpolarized scattering on spin one-half objects, the first structure dependent contributions in this energy expansion of the amplitude are the electric polarizability, α, and the magnetic polarizability, β. These quantities reflect the ability of the hadron's components to align or antialign themselves in response to an applied electric or magnetic field. For the proton and neutron, the positivity of the accepted experimental values of these polarizabilities ($\alpha_p = 12.0 \pm 0.6$, $\beta_p = 1.9 \mp 0.6$, $\alpha_n = 12.5 \pm 1.7$ and $\beta_n = 2.7 \mp 1.8$ in units of 10^{-4} fm^3 [1]) indicates that both nucleons are diamagnetic objects. Recent experimental advances [1,2] have also allowed the extraction of certain combinations of target polarization-dependent observables in Compton scattering. These involve the so-called spin polarizabilities [3], conventionally labeled γ_1–γ_4, and they have consequently been investigated in numerous theoretical and further experimental studies. Although the classical interpretation of spin-dependent Compton scattering is less clear, the spin polarizabilities encode additional fundamental properties of the nucleon. Compton scattering observables, however, are not limited to these six parameters. Higher-order quasistatic properties of the nucleon appear from further terms in the energy expansion of the amplitude. These higher-order polarizabilities [4], as well as generalized polarizabilities [5] (which arise in the singly (doubly) virtual Compton scattering process, $\gamma^* X \to \gamma^{(*)} X$) allow for an even finer resolution of the electromagnetic structure of hadrons at low energies.

While experimentally one is hoping to open further windows through which to view hadronic electromagnetic structure, theoretically one ultimately hopes to understand how hadronic polarizabilities arise from the basic electromagnetic interaction of the photon with quarks that are bound to form the hadrons. The electric and magnetic polarizabilities should naïvely scale with the volume of the hadron. However, this expectation overestimates the observed polarizabilities by four orders of magnitude, indicating that the nucleon's constituents are strongly coupled. Lattice techniques provide a method to investigate the nonperturbative structure of hadrons directly from QCD. In particular, the various hadron polarizabilities can be computed. Comparison of these results with experimental determinations would provide stringent tests of the lattice method's ability to reproduce the structure of physical hadronic states; for the individual spin polarizabilities that have not been measured, the lattice approach may be the only way to determine them. On the lattice, direct calculations of the required hadronic current-current correlators are difficult and so far have not been attempted. However significant progress has been made [6–8] in extracting the electric and magnetic polarizabilities by performing quenched lattice calculations in constant background electric and magnetic fields, respectively, and studying the quadratic shift in the hadron mass that is induced (essentially an application of the Feynman-Hellman theorem). These studies have investigated the electric polarizabilities of various neutral hadrons (in particular, the uncharged vector mesons and uncharged octet and decuplet baryons), and the magnetic polarizabilities of the baryon octet and decuplet, as well as those of the nonsinglet pseudoscalar and vector mesons. As we shall discuss below, generalisations of these methods using nonconstant fields allow the extraction of the spin polarizabilities from spin-dependent correlation functions and also allow the electric polarizabilities to be determined for charged hadrons. More generally, higher-order polarizabil-

*Electronic address: wdetmold@phys.washington.edu
†Electronic address: bctiburz@phy.duke.edu
‡Electronic address: walkloud@u.washington.edu

ities and generalized polarizabilities are accessible using this technique.

As with all current lattice results, these calculations have a number of limitations and so are not physical predictions that can be directly compared to experiment. For the foreseeable future, lattice QCD calculations will necessarily use quark masses that are larger than those in nature because of limitations in the available algorithms and computational power. Additionally, the volumes and lattice-spacings used in these calculations will always be finite and nonvanishing, respectively. For sufficiently small masses and large volumes, the effects of these approximations can be investigated systematically using the effective field theory of the low-energy dynamics of QCD, chiral perturbation theory (χPT) [9–11].[1] In this paper we shall perform an analysis of the nucleon electromagnetic and spin polarizabilities at next-to-leading order (NLO) in the chiral expansion. We do so to discuss the infrared effects of the quark masses and finite volume in two-flavor QCD and its quenched and partially-quenched analogues (QQCD and PQQCD). The polarizabilities of the hadrons are particularly interesting in this regard since they are very sensitive to infrared physics and their quark mass and finite volume dependence is considerably stronger than that expected for hadron masses and magnetic moments. This should be physically evident given that the polarizabilities scale with the volume. In essence, chiral perturbation theory provides a model independent analysis of the modification of the nucleon's pion cloud in a finite volume. When the charged pion cloud is influenced by to the periodic boundary conditions imposed on the lattice, the nucleon's response to external electromagnetic fields is altered compared to that at infinite volume, and in most cases the effects are dramatic. A particularly striking oddity that we find in this analysis is a modification of the Thompson cross section at finite volume. This can be explained through the physics of chiral loop corrections to pointlike hadron structure.

If future lattice QCD simulations are to provide physical predictions for the electromagnetic and spin polarizabilities, careful attention must be paid to both the chiral and infinite volume extrapolations. To illustrate this point, we present our results at representative values of the quark mass, finding significant effects. We also use our quenched chiral perturbation theory results to assess the volume dependence of the quenched data at the lightest pion masses used in Refs. [7,8]. While the quenched theory contains unphysical low energy constants (LECs) and the convergence of the chiral expansion is questionable at these pion masses, we can still provide an estimate of the volume dependence of quenched data for the nucleon polarizabilities using our results. Such an estimate is achievable because the corresponding polarizabilities in the unquenched theory do not depend on phenomenologically undetermined LECs at the order of the chiral expansion to which we work. At the lightest quark masses used in the existing quenched lattice simulations, $m_\pi \sim 0.5$ GeV, we find strong sensitivity to the lattice volume (as large as 10%). The effects will only increase as the pion mass is brought closer to that in nature. Clearly careful chiral and volume extrapolations of polarizabilities are mandated to connect lattice calculations to real world QCD.

To begin our investigation of nucleon polarizabilities in lattice QCD, we discuss in Sec. II the kinematics of Compton scattering and define the electromagnetic and spin polarizabilities that are the primary focus of this work. In Sec. III, we perform a general analysis of the external field method pertaining to all electromagnetic and spin polarizabilities. We discuss how suitable background fields can be used in lattice QCD simulations to determine the spin polarizabilities and, more generally, generalized polarizabilities (though we limit our discussion of these in the present paper). Following this we introduce the low-energy effective theories of QCD (χPT), quenched QCD (QχPT) and partially-quenched QCD (PQχPT). These effective theories provide the model independent input necessary for calculating the quark mass and lattice volume dependence of polarizabilities. We focus primarily on PQχPT in Sec. IV, discussing the relation to χPT where relevant, and relegating the peculiarities of QχPT to Appendix A. Our results for the dependence of the nucleon polarizabilities on quark masses and the lattice volume are presented in Sec. V. We provide detailed plots relevant for full QCD simulations of polarizabilities showing the dependence on quark masses and lattice volumes. We also estimate the quenched QCD volume dependences of the polarizabilities at a pion mass typical of existing quenched lattice data. Very small volumes are discussed in Appendix B and a glossary of finite volume functions required to evaluate the polarizabilities in a periodic box appears in Appendix C. Lastly, Sec. VI consists of a concluding discussion of our results.

II. COMPTON SCATTERING ON SPIN-HALF HADRONS

The real Compton scattering amplitude describing the elastic scattering of a photon on a spin-half target such as the proton or neutron can be parametrized as

$$\begin{aligned} T_{\gamma N} = {} & A_1(\omega,\theta)\vec{\epsilon}\,'\cdot\vec{\epsilon} + A_2(\omega,\theta)\vec{\epsilon}\,'\cdot\hat{k}\,\vec{\epsilon}\cdot\hat{k}' \\ & + iA_3(\omega,\theta)\vec{\sigma}\cdot(\vec{\epsilon}\,'\times\vec{\epsilon}) + iA_4(\omega,\theta)\vec{\sigma}\cdot(\hat{k}'\times\hat{k})\vec{\epsilon}\,'\cdot\vec{\epsilon} \\ & + iA_5(\omega,\theta)\vec{\sigma}\cdot[(\vec{\epsilon}\,'\times\hat{k})\vec{\epsilon}\cdot\hat{k}' - (\vec{\epsilon}\times\hat{k}')\vec{\epsilon}\,'\cdot\hat{k}] \\ & + iA_6(\omega,\theta)\vec{\sigma}\cdot[(\vec{\epsilon}\,'\times\hat{k}')\vec{\epsilon}\cdot\hat{k}' - (\vec{\epsilon}\times\hat{k})\vec{\epsilon}\,'\cdot\hat{k}], \end{aligned} \tag{1}$$

[1]The effects of the lattice discretization are short distance in nature, and while some of them can be analyzed in an extension of the effective field theory described here [12–15], others are not accounted for. Here we will assume that a continuum extrapolation has been performed.

where we have chosen to work in the Breit frame of the system and the incoming and outgoing photons have momenta $k = (\omega, \vec{k} = \omega\hat{k})$ and $k' = (\omega, \vec{k}' = \omega\hat{k}')$, and polarization vectors ϵ and ϵ', respectively. The $A_i(\omega, \theta)$, $i = 1 \ldots 6$, are scalar functions of the photon energy and scattering angle, $\cos\theta = \hat{k} \cdot \hat{k}'$. It is convenient to work in Coulomb gauge throughout where $\epsilon_0 = \epsilon'_0 = 0$ (the physical amplitudes are gauge invariant).

The functions, A_i, determining the Compton amplitude can be separated into a number of pieces. The Born terms describe the interaction of the photon with a pointlike target with mass, M_N, charge, eZ (where $e > 0$), and magnetic moment, μ. These terms reproduce the Thomson-limit and quadratic frequency pieces [16] of unpolarized scattering and the Low–Gell-Mann–Goldberger low energy theorems [17,18] for spin-dependent scattering. The remaining parts of the amplitude describe the structural response of the target. Expanding the amplitude for small photon energies relative to the target mass and keeping terms to $\mathcal{O}(\omega^3)$ one can write

$$\begin{aligned}
A_1(\omega, \theta) &= -Z^2 \frac{e^2}{M_N} + \frac{e^2}{4M_N^3}(\mu^2(1 + \cos\theta) - Z^2) \\
&\quad \times (1 - \cos\theta)\omega^2 + 4\pi(\alpha + \beta\cos\theta)\omega^2 + \mathcal{O}(\omega^4), \\
A_2(\omega, \theta) &= \frac{e^2}{4M_N^3}(\mu^2 - Z^2)\omega^2\cos\theta - 4\pi\beta\omega^2 + \mathcal{O}(\omega^4), \\
A_3(\omega, \theta) &= \frac{e^2\omega}{2M_N^2}(Z(2\mu - Z) - \mu^2\cos\theta) \\
&\quad + 4\pi\omega^3(\gamma_1 - (\gamma_2 + 2\gamma_4)\cos\theta) + \mathcal{O}(\omega^5), \qquad (2) \\
A_4(\omega, \theta) &= -\frac{e^2\omega}{2M_N^2}\mu^2 + 4\pi\omega^3\gamma_2 + \mathcal{O}(\omega^5), \\
A_5(\omega, \theta) &= \frac{e^2\omega}{2M_N^2}\mu^2 + 4\pi\omega^3\gamma_4 + \mathcal{O}(\omega^5), \\
A_6(\omega, \theta) &= -\frac{e^2\omega}{2M_N^2}Z\mu + 4\pi\omega^3\gamma_3 + \mathcal{O}(\omega^5),
\end{aligned}$$

describing the target structure in terms of the electric, magnetic and four spin polarizabilities, α, β, and γ_{1-4}, respectively. In the conventions above, the spin polarizabilities receive contributions from the anomalous decay $\pi^0 \to \gamma\gamma$ (see Sec. VA 1). This contribution varies rapidly with energy and is omitted from the polarizabilities in some conventions. Higher-order terms in the energy expansion can be parametrized in terms of higher-order polarizabilities [4]. The more general process of virtual (and doubly-virtual) Compton scattering at low energies can similarly be described in terms of generalized polarizabilities [5]. We will focus on the six polarizabilities defined above.

The goal of this paper is to determine the quark mass and volume dependence of the polarizabilities defined above to allow accurate extraction of their physical values from lattice calculations. Before we do this we shall discuss how these lattice calculations may be implemented.

III. COMPTON SCATTERING AND POLARIZABILITIES ON THE LATTICE

Lattice QCD provides a way to study the polarizabilities of hadrons from first principles. There are two ways to do this. The method most reminiscent of the experimental situation is to study the (Euclidean space) four-point Green function defining the Compton scattering tensor directly (the photon fields are amputated). By measuring the large Euclidean time behavior of this correlator, the hadron matrix elements of the two vector currents can be extracted. In principle, by calculating particular Lorentz components of the Compton tensor with various different source and sink spin states, all six electromagnetic and spin polarizabilities and their higher-order and generalized analogues can be extracted. However, this is a complicated task, requiring the evaluation a large number of quark propagator contractions resulting from quarkline disconnected diagrams which are statistically difficult to determine. At present this approach is too demanding for the available computational resources and has not been attempted.

The second method is based on measuring the response of hadronic states to fixed external fields. A number of exploratory quenched QCD studies have been performed in this approach. The pioneering calculations of Refs. [19–24] attempted to measure the nucleon axial couplings, magnetic moments and electric dipole moments by measuring the linear shift in the hadron energy as a function of an applied external weak or electromagnetic field. As discussed in the Introduction, various groups [6–8,25] have also used this approach to extract electric and magnetic polarizabilities in quenched QCD by measuring a quadratic shift in the hadron energy in external electric and magnetic fields. The method is not limited to electroweak external fields and can be used to extract many matrix elements such as those that determine the moments of parton distributions and the total quark contribution to the spin of the proton [26]. Here we focus on the electromagnetic case.

The Euclidean space ($x_4 \equiv \tau$) effective action describing the gauge and parity invariant interactions of a nonrelativistic spin-half hadron of mass M and charge q with a classical U(1) gauge field, $A^\mu(\vec{x}, \tau)$, is

$$S_{\text{eff}}[A] = \int d^3x d\tau \mathcal{L}_{\text{eff}}(\vec{x}, \tau; A), \qquad (3)$$

for the Lagrangian

$$\mathcal{L}_{\rm eff}(\vec{x},\tau;A) = \Psi^\dagger(\vec{x},\tau)\Big[\Big(\frac{\partial}{\partial\tau} + iqA_4\Big) + \frac{(-i\vec{\nabla} - q\vec{A})^2}{2M} - \mu\vec{\sigma}\cdot\vec{H} + 2\pi(\alpha\vec{E}^2 - \beta\vec{H}^2) - 2\pi i(-\gamma_{E_1E_1}\vec{\sigma}\cdot\vec{E}\times\dot{\vec{E}} + \gamma_{M_1M_1}\vec{\sigma}\cdot\vec{H}\times\dot{\vec{H}} + \gamma_{M_1E_2}\sigma^i E^{ij}H^j + \gamma_{E_1M_2}\sigma^i H^{ij}E^j)\Big]\Psi(\vec{x},\tau) + \ldots, \quad (4)$$

where $\vec{E} = -\frac{\partial}{\partial\tau}\vec{A}(\vec{x},\tau) - \vec{\nabla}A_4(\vec{x},\tau)$ and $\vec{H} = \vec{\nabla}\times\vec{A}(\vec{x},\tau)$ are the corresponding electric and magnetic fields, $\dot{X} = \frac{\partial}{\partial\tau}X$ denotes the Euclidean time derivative, $X^{ij} = \frac{1}{2}\times(\partial^i X^j + \partial^j X^i)$, and the ellipsis denotes terms involving higher dimensional operators. By calculating one- and two-photon processes with this effective Lagrangian, it is clear that the constants that appear in Eq. (4) are indeed the relevant magnetic moment and electromagnetic and multipole polarizabilities [27] [these are simply related to the polarizabilities defined in the previous section as: $\gamma_{E_1E_1} = -(\gamma_1+\gamma_3)$, $\gamma_{M_1M_1} = \gamma_4$, $\gamma_{E_1M_2} = \gamma_3$ and $\gamma_{M_1E_2} = \gamma_2 + \gamma_4$]. The Schrödinger equation corresponding to Eq. (4) determines the energy of the particle in an external U(1) field in terms of the charge, magnetic moment, and polarizabilities. Higher-order terms in Eq. (4) (which contain in part the higher-order polarizabilities [4]) can be neglected for sufficiently weak external fields. For a magnetic field, the minimally coupled terms generate towers of Landau levels and for a constant electric field the same terms accelerate charged particles.

Lattice calculations of the energy of a hadron in an external U(1) field are straight-forward. One measures the behavior of the usual two-point correlator on an ensemble of gauge configurations generated in the presence of the external field. This changes the Boltzmann weight used in selecting the field configurations from $\det[\not{D} + m]\exp[-S_g]$ to $\det[\not{D} + i\hat{Q}\not{A} + m]\exp[-S_g]$, where $\not{D}$ is the SU(3) gauge covariant derivative, $\hat{Q}$ is the quark electromagnetic charge operator, and S_g is the usual SU(3) gauge action. Since calculations are required at a number of different values of the field strength in order to correctly identify shifts in energy from the external field, this is a relatively demanding computational task (although it is at least conceptually simpler than studying the four-point function). In general one must worry about the positivity of the fermionic determinant calculated in the presence of a background field, however for weak fields, positivity is preserved. The exploratory studies of Refs. [6–8,19–25] used quenched QCD in which the gluon configurations do not feel the presence of the U(1) field as the quark determinant is absent. In this case, the external field can be applied after the gauge configurations had been generated and is simply implemented by multiplying the SU(3) gauge links of each configuration by link variables corresponding to the fixed external field: $\{U^\mu_\alpha(x)\} \to \{U^\mu_\alpha(x)\exp[ieaA^\mu]\}$, where a is the lattice spacing. These studies are interesting in that they provide a proof of the method, however the values of the polarizabilities extracted have no connection to those measured in experiment.

It is clear from Eq. (4) that all six polarizabilities can be extracted using suitable space and time varying background fields if the shift of the hadron energy at second order in the strength of the field can be determined. One can also see this because the Compton tensor appears explicitly as the second-order connected term in the expansion of hadronic two-point correlation function in weak background fields [26]. Previous studies [6–8,25] have employed constant electric and magnetic fields to determine the corresponding polarizabilities in quenched QCD. Here we perform a more general analysis to show how the spin polarizabilities and the electric polarizabilities of charged particles can be obtained.

In order to determine the polarizabilities, we consider lattice calculations of the two-point correlation function

$$C_{ss'}(\vec{p},\tau;A) = \int d^3x e^{i\vec{p}\cdot\vec{x}}\langle 0|\chi_s(\vec{x},\tau)\chi^\dagger_{s'}(0,0)|0\rangle_A, \quad (5)$$

where $\chi_s(\vec{x},\tau)$ is an interpolating field with the quantum numbers of the hadron under consideration (we will focus on the nucleons) with z component of spin, s, and the correlator is evaluated on the ensemble of gauge configurations generated with the external field, A^μ.

For uncharged hadrons at rest in constant electric and magnetic fields, it is simple to show that this correlator falls off exponentially at large times with an energy given by the appropriate terms in Eq. (4) owing to the constancy of the effective Hamiltonian. However for space-time varying fields, charged particles or states of nonzero $\vec{p}$, a more general analysis is needed. This is most easily formulated using the effective field theory (EFT) defined by Eq. (4). For weak external fields (such that higher-order terms in Eq. (4) can be safely neglected), the small $\vec{p}$ and large τ dependence of this QCD correlation function is reproduced by the equivalent correlator calculated in the effective theory corresponding to the Lagrangian, Eq. (4). That is

$$C_{ss'}(\vec{p},\tau;A) = \int d^3x e^{i\vec{p}\cdot\vec{x}}\frac{1}{\mathcal{Z}_{\rm eff}[A]} \times \int \mathcal{D}\Psi^\dagger\mathcal{D}\Psi\Psi_s(\vec{x},\tau)\Psi^\dagger_{s'}(0,0) \times \exp(-S_{\rm eff}[A]), \quad (6)$$

where $\mathcal{Z}_{\rm eff}[A] = \int\mathcal{D}\Psi^\dagger\mathcal{D}\Psi\exp(-S_{\rm eff}[A])$. Since the right-hand side of Eq. (6) is completely determined in terms of the charge, magnetic moment and polarizabilities that we seek to extract, fitting lattice calculations of $C_{ss'}(\vec{p},\tau;A)$ in a given external field to the effective field theory expression will enable us to determine the appropriate polarizabilities. In the above equation we have assumed that the ground state hadron dominates the

correlator at the relevant times. For weak fields this will be the case. However one can consider additional terms in the effective Lagrangian that describe the low excitations of the hadron spectrum that have the same quantum numbers as the hadron under study. This will lead to additive terms in Eq. (6) that depend on the mass, magnetic moment and polarizabilities of the excited hadron instead of those of the ground state. With precise lattice data, the properties of these excited states can also be determined.

In many simple cases such as constant or plane-wave external fields, the EFT version of $C_{ss'}(\vec{p}, \tau; A)$ can be determined analytically in the infinite volume, continuum limit [28]. However in finite lattice spacing and at finite volume, calculating $C_{ss'}(\vec{p}, \tau; A)$ in the EFT becomes more complicated. In order to determine the EFT correlator, we must invert the matrix $\mathcal{K}$ defined by

$$S_{\text{latt}}[A] = \sum_{\vec{x},\tau_x} \sum_{\vec{y},\tau_y} \sum_{s,s'} \Psi_s^\dagger(\vec{x}, \tau_x) \mathcal{K}_{ss'}[\vec{x}, \tau_x, \vec{y}, \tau_y; A] \Psi_s(\vec{y}, \tau_y), \tag{7}$$

where $S_{\text{latt}}[A]$ is a discretization of the EFT action in which derivatives are replaced by finite differences (the time derivative is given by a forward difference as we can ignore antiparticles). $\mathcal{K}$ has dimension $4N_l^2$ where N_l is the number of lattice sites. For the most general space-time varying external field, this must be inverted numerically; given a set of lattice results for the correlator, Eq. (6) is repeatedly evaluated for varying values of the polarizabilities until a good description of the lattice data is obtained.

For weak fields such that $|A^\mu(\vec{x}, \tau)|^2 \ll \Lambda_{\text{QCD}}^2$ for all $\vec{x}$ and τ, a perturbative expansion of $\mathcal{K}^{-1}$ in powers of the field can be used. This corresponds to the series of diagrams in Fig. 1. To extract all six polarizabilities using such an analysis, we need to consider a number of different fields; lattice calculations of the correlators in Eq. (5) using

$$A^\mu_{(1)}(x) = \begin{pmatrix} ia_1\tau \\ 0 \\ 0 \\ 0 \end{pmatrix}, \qquad A^\mu_{(2)}(x) = \begin{pmatrix} -\frac{a_2}{2}x_2 \\ \frac{a_2}{2}x_1 \\ 0 \\ 0 \end{pmatrix},$$

$$A^\mu_{(3)}(x) = \begin{pmatrix} 0 \\ -\frac{i}{a}a_3\tau x_3 \\ -b_3 x_1 \\ 0 \end{pmatrix}, \qquad A^\mu_{(4)}(x) = \begin{pmatrix} -\frac{i}{a}a_4\tau x_2 \\ 0 \\ -\frac{1}{2}b_4 x_1 \\ 0 \end{pmatrix}, \tag{8}$$

$$A^\mu_{(5)}(x) = \begin{pmatrix} \frac{1}{a}a_5 x_2 x_1 \\ \frac{1}{2a}a_5 x_2^2 \\ ib_5\tau \\ 0 \end{pmatrix}, \qquad A^\mu_{(6)}(x) = \begin{pmatrix} -\frac{1}{2a}a_6\tau^2 \\ -i\frac{1}{2}b_6\tau \\ 0 \\ 0 \end{pmatrix},$$

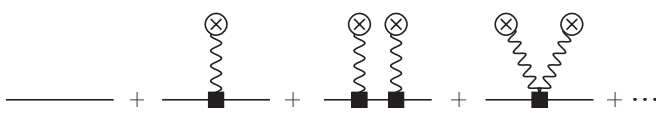

FIG. 1. Perturbative expansion of the hadron propagator in an external field.

for a number of different choices for the strength parameters, a_i and b_i (with $|a_i|, |b_i| \ll \Lambda_{\text{QCD}}^2$), are sufficient to determine the full set of polarizabilities.[2] By measuring correlators for different spin configurations (including those that flip spin), we can reduce the number of fields required to extract the polarizabilities.

As an example, the behavior of the correlator in the field $A^\mu_{(1)}(x)$ (which corresponds to a constant electric field in the x_1 direction) is given by

$$\begin{aligned} C_{ss'}(\vec{p}, \tau; A_{(1)}) &= \delta_{s,s'} \exp\Big\{ -\frac{a_1\tau}{6M}[a_1(q^2\tau^2 + 12M\pi\alpha) \\ &\quad - 3iq\tau p_1]\Big\} e^{-M\tau} e^{-(\tau/2M)|\vec{p}|^2} + \mathcal{O}(a_1^3) \\ &\xrightarrow{|\vec{p}|\to 0} \delta_{s,s'} \exp\Big[-(M + 2\pi\alpha a_1^2)\tau - \frac{q^2 a_1^2}{6M}\tau^3 \Big] \\ &\quad + \mathcal{O}(a_1^3). \end{aligned} \tag{9}$$

In this case, the perturbative series has been resummed exactly in the continuum, infinite volume limit and the higher-order corrections come from terms omitted in Eq. (4). For electrically neutral particles, the exponential falloff of this correlator determines the polarizability α once the mass M has been measured in the zero-field case. When a charged particle is placed in such a field it undergoes continuous acceleration in the x_1 direction (this is described by the τ^3 term in the exponent). However at times small compared to $\sqrt{6M}/qa_1$, the correlator essentially falls off exponentially. Matching the behavior of Eq. (9) to lattice data for a charged hadron will again enable us to determine the electric polarizability, α.

As a second analytic example, we consider one of the multipole polarizabilities. In the presence of the field $A^\mu_{(6)}(x)$, which corresponds to a more complicated electric field $\vec{E}_{(6)}(x) = (\frac{a_6}{a}\tau, i\frac{b_6}{2}, 0)$, we find that

$$\frac{C_{\uparrow\uparrow}(\vec{p}, \tau; A_{(6)})}{C_{\downarrow\downarrow}(\vec{p}, \tau; A_{(6)})} = \exp\Big[\frac{2\pi}{a} a_6 b_6 \gamma_{E_1E_1}\tau\Big] + \ldots, \tag{10}$$

independent of $\vec{p}$ and the ellipsis denotes terms cubic in the field that have been neglected in Eq. (4). Whilst the individual correlators, $C_{\uparrow\uparrow}$ and $C_{\downarrow\downarrow}$, have relatively complicated time-momentum behavior involving q and α as well as $\gamma_{E_1E_1}$, this becomes very simple in the ratio and $\gamma_{E_1E_1}$ can be determined cleanly.

Analogous results can be derived for the other fields in Eq. (8), however to take into account the finite lattice spacing and periodic finite volume nature of the underlying

[2]These fields correspond to real $\vec{E}$ and $\vec{H}$ fields in Minkowski-space for real-valued a_i and b_i. Since periodic spatial boundary conditions are envisaged for the link variables, there are quantisation conditions that must be satisfied by the a_i [20,21]. For example, $q_i a_2 = 2\pi n/aL$ for each of the quark charges q_i. The more complicated fields in Eq. (8) require two parameters to satisfy these conditions.

lattice simulations to which the EFT description is matched, the correlator is most easily calculated by inverting the matrix $\mathcal{K}$ numerically. This also allows for more general choices of fields. If we seek to extract higher-order polarizabilities, the Lagrangian in Eq. (4) must be extended to include higher dimension operators [4]. At this order, relativistic corrections and three-photon couplings also need to be included. Correlation functions similar to those in Eq. (6) involving two different external momenta will allow us to also extract the generalized polarizabilities [5].

IV. HEAVY BARYON χPT

To calculate the quark mass and volume dependence of the nucleon polarizabilities, we use heavy baryon chiral perturbation theory (HBχPT) as was first constructed in Refs. [29–32]. In current lattice calculations, valence and sea quarks are often treated differently, with sea quarks either absent (quenched QCD) or having different masses than the valence quarks (partially-quenched QCD).[3] The extensions of HBχPT to quenched HBχPT [35,36] and partially-quenched HBχPT [37,38] to accommodate these modifications are also well established and have been used to calculate many baryon properties. In this section, we will primarily focus on the two-flavor partially-quenched theory and briefly introduce the relevant details following the conventions set out in Ref. [38]. Since QCD is a special limit of the partially-quenched theory, our discussion also encompasses two-flavor χPT. Additional complications in quenched χPT are relegated to Appendix A.

A. Pseudo-Goldstone mesons

We consider a partially-quenched theory of valence (u, d), sea (j, l) and ghost $(\tilde{u}, \tilde{d})$ quarks with masses contained in the matrix

$$m_Q = \mathrm{diag}(m_u, m_d, m_j, m_l, m_{\tilde{u}}, m_{\tilde{d}}), \tag{11}$$

where $m_{\tilde{u},\tilde{d}} = m_{u,d}$ such that the path-integral determinants arising from the valence and ghost-quark sectors exactly cancel. The corresponding low-energy meson dynamics are described by the PQχPT Lagrangian. At leading order this is given by

$$\mathcal{L}_\Phi = \frac{f^2}{8}\,\mathrm{str}[\mathcal{D}^\mu\Sigma^\dagger\mathcal{D}_\mu\Sigma] + \lambda\frac{f^2}{4}\,\mathrm{str}[m_Q\Sigma^\dagger + m_Q^\dagger\Sigma] + \alpha_\Phi\mathcal{D}^\mu\Phi_0\mathcal{D}_\mu\Phi_0 - m_0^2\Phi_0^2, \tag{12}$$

where the pseudo-Goldstone mesons are embedded nonlinearly in

$$\Sigma = \xi^2 = \exp\left(\frac{2i\Phi}{f}\right), \tag{13}$$

with the matrix Φ given by

$$\Phi = \begin{pmatrix} M & \chi^\dagger \\ \chi & \tilde{M} \end{pmatrix}, \tag{14}$$

and

$$M = \begin{pmatrix} \eta_u & \pi^+ & \phi_{uj} & \phi_{ul} \\ \pi^- & \eta_d & \phi_{dj} & \phi_{dl} \\ \phi_{ju} & \phi_{jd} & \eta_j & \phi_{jl} \\ \phi_{lu} & \phi_{ld} & \phi_{lj} & \eta_l \end{pmatrix}, \qquad \tilde{M} = \begin{pmatrix} \tilde{\eta}_u & \tilde{\pi}^+ \\ \tilde{\pi}^- & \tilde{\eta}_d \end{pmatrix},$$
$$\chi = \begin{pmatrix} \phi_{\tilde{u}u} & \phi_{\tilde{u}d} & \phi_{\tilde{u}j} & \phi_{\tilde{u}l} \\ \phi_{\tilde{d}u} & \phi_{\tilde{d}d} & \phi_{\tilde{d}j} & \phi_{\tilde{d}l} \end{pmatrix}, \tag{15}$$

and where $\Phi_0 = \mathrm{str}(\Phi)/\sqrt{2}$. The upper left 2×2 block of M corresponds to the usual valence-valence mesons, the lower right to sea-sea mesons and the remaining entries of M to valence-sea mesons. Mesons in $\tilde{M}$ are composed of ghost quarks and ghost antiquarks and thus bosonic. Mesons in χ contain ghost-valence or ghost–sea-quark–antiquark pairs and are fermionic. In terms of the quark masses, the tree-level meson masses are given by

$$m_{\Phi_{ij}}^2 = m_{Q_iQ_j}^2 = \lambda[(m_Q)_{ii} + (m_Q)_{jj}], \tag{16}$$

where $Q = (u, d, j, l, \tilde{u}, \tilde{d})$. The terms proportional to α_Φ and m_0 in Eq. (12) involve the flavor-singlet field and are only relevant in the quenched theory (see Appendix A); in both PQχPT and χPT the singlet meson acquires a large mass through the strong $\mathrm{U}(1)_A$ anomaly and can be integrated out, leading to a modified flavor-neutral propagator that contains both single and double pole structures [39].

In the above Lagrangian, we have minimally coupled electromagnetism (the U(1) gauge field is again denoted by A^μ and its field strength tensor $F^{\mu\nu} = \partial^\mu A^\nu - \partial^\nu A^\mu$) to the theory through the chiral, and U(1) gauge covariant derivative

$$\mathcal{D}^\mu = \partial^\mu + [\mathcal{V}^\mu, \quad], \tag{17}$$

with the vector current

$$\mathcal{V}^\mu = \tfrac{1}{2}[\xi(\partial^\mu - ie\mathcal{Q}A^\mu)\xi^\dagger + \xi^\dagger(\partial^\mu - ie\mathcal{Q}A^\mu)\xi], \tag{18}$$

depending on the quark charge matrix, $\mathcal{Q}$. In coupling electromagnetism to this theory, we must specify how the quark charges are extended to the partially-quenched theory. We choose:

$$\mathcal{Q} = \mathrm{diag}(q_u, q_d, q_j, q_l, q_u, q_d), \tag{19}$$

though other arrangements are possible. However, one

[3] At finite lattice spacing, different actions can even be used for the different quark sectors (e.g., staggered sea quarks and domain wall valence quarks). As was shown in Refs. [15,33,34], the lattice spacing corrections to baryon electromagnetic properties are expected to be small, as they can not enter at tree level, and for current simulations with $a\Lambda_{\mathrm{QCD}}^2 \sim m_q$, they generally enter at leading loop order through valence-sea meson masses. In our work we assume a continuum extrapolation has been performed.

must set $q_j + q_l \neq 0$ in order to retain sensitivity to the full set of LECs that appear in two-flavor χPT [40,41]. In addition to the Lagrangian, Eq. (12), the anomalous couplings of the Wess-Zumino-Witten Lagrangian [42,43] will also contribute to the spin polarizabilities. These terms are described below.

B. Baryons

In SU(4|2) HBχPT, the physical nucleons (those composed of three valence quarks) are embedded in a **70**-dimensional representation of the flavor group described by a three index flavor-tensor, $\mathcal{B}$ [37,38]. Since the mass-splitting between the nucleon and Δ-isobar, $\Delta = M_\Delta - M_N \sim 300$ MeV, is comparable to the physical pion mass (and less than pion masses used in current lattice simulations), the Δ-isobar must be included in the theory. These fields are represented in a totally symmetric three index flavor-tensor $\mathcal{T}^\mu$ (a Rarita-Schwinger field) transforming as a **44**-dimensional representation of SU(4|2). The mass-splitting Δ is small compared to the chiral symmetry breaking scale, and in this work we treat $\Delta \sim m_\pi$ in the power counting [30]. For additional details, see Refs. [35,37,38].

The relevant part of leading-order Lagrangian describing these baryons and their interactions with Goldstone mesons is

$$\begin{aligned}\mathcal{L}_B^{(0)} &= i(\bar{\mathcal{B}} v\cdot\mathcal{D}\mathcal{B}) - i(\bar{\mathcal{T}}^\mu v\cdot\mathcal{D}\mathcal{T}_\mu) + \Delta(\bar{\mathcal{T}}^\mu\mathcal{T}_\mu)\\ &\quad + 2\alpha(\bar{\mathcal{B}}S^\mu\mathcal{B}\mathcal{A}_\mu) + 2\beta(\bar{\mathcal{B}}S^\mu\mathcal{A}_\mu\mathcal{B})\\ &\quad + 2\mathcal{H}(\bar{\mathcal{T}}^\nu S^\mu\mathcal{A}_\mu\mathcal{T}_\nu) + \sqrt{\frac{3}{2}}\mathcal{C}[(\bar{\mathcal{T}}^\nu\mathcal{A}_\nu\mathcal{B})\\ &\quad + (\bar{\mathcal{B}}\mathcal{A}_\nu\mathcal{T}^\nu)],\end{aligned} \tag{20}$$

where v^μ is the baryon velocity, S^μ is the covariant spin-vector [29,31] and $\mathcal{D}^\mu$ is the chiral, and U(1) covariant derivative [35]. The axial-vector current is given by

$$\mathcal{A}^\mu = \frac{i}{2}[\xi(\partial^\mu - ie\mathcal{Q}A^\mu)\xi^\dagger - \xi^\dagger(\partial^\mu - ie\mathcal{Q}A^\mu)\xi]. \tag{21}$$

The various flavor contractions (indicated by the parentheses) are defined as in Ref. [38]. In order for $\mathcal{T}^\mu$ to correctly describe the spin-3/2 sector, the constraints $v\cdot\mathcal{T} = S\cdot\mathcal{T} = 0$ are used. The partially-quenched Lagrangian, Eq. (20), contains one more operator than the corresponding two-flavor χPT Lagrangian. To determine the relation of the partially-quenched operators to those of SU(2) χPT, one simply restricts the flavor indices of all the operators in Eq. (20) to the valence sector, leading to

$$\begin{aligned}\alpha &= \tfrac{4}{3}g_A + \tfrac{1}{3}g_1, \qquad \beta = \tfrac{2}{3}g_1 - \tfrac{1}{3}g_A,\\ \mathcal{C} &= -g_{\Delta N}, \qquad \mathcal{H} = g_{\Delta\Delta}.\end{aligned} \tag{22}$$

Here, g_1 is the coupling of the nucleons to the SU(2) singlet-meson field, which decouples in χPT. Thus when the QCD limit of the partially-quenched theory is taken, where $m_j = m_u$ and $m_l = m_d$, all dependence on g_1 vanishes (in the quenched theory, quantities may still depend on this parameter, see Appendix A).

As with the mesons, at leading order the photon is minimally coupled to the baryons with fixed coefficients. At the next order in the expansion there are a number of new electromagnetic gauge invariant operators which contribute to the Compton amplitude and the polarizabilities. Here, we display the relevant terms at this order,

$$\begin{aligned}\mathcal{L}_B^{(1)} &= \frac{ie}{2M_N}F_{\mu\nu}[\mu_\alpha(\bar{\mathcal{B}}[S^\mu, S^\nu]\mathcal{B}\mathcal{Q}_{\xi+})\\ &\quad + \mu_\beta(\bar{\mathcal{B}}[S^\mu, S^\nu]\mathcal{Q}_{\xi+}\mathcal{B})\\ &\quad + \mu_\gamma\,\mathrm{str}[\mathcal{Q}_{\xi+}](\bar{\mathcal{B}}[S^\mu, S^\nu]\mathcal{B})]\\ &\quad + \sqrt{\frac{3}{2}}\mu_T\frac{ie}{2M_N}F_{\mu\nu}[(\bar{\mathcal{B}}S^\mu\mathcal{Q}_{\xi+}\mathcal{T}^\nu)\\ &\quad + (\bar{\mathcal{T}}^\mu S^\nu\mathcal{Q}_{\xi+}\mathcal{B})],\end{aligned} \tag{23}$$

where $\mu_{\alpha,\beta,\gamma}$ are magnetic moment coefficients [36,38], μ_T is the coefficient of the M1 transition **70**–**44** operator [33,44] and

$$\mathcal{Q}_{\xi^\pm} = \tfrac{1}{2}(\xi^\dagger\mathcal{Q}\xi \pm \xi\mathcal{Q}\xi^\dagger). \tag{24}$$

The partially-quenched magnetic moment coefficients are related to the isoscalar and isovector magnetic coefficients, μ_0 and μ_1, in standard two-flavor χPT as

$$\mu_0 = \tfrac{1}{6}(\mu_\alpha + \mu_\beta + 2\mu_\gamma), \qquad \mu_1 = \tfrac{1}{6}(2\mu_\alpha - \mu_\beta), \tag{25}$$

where the χPT Lagrangian describing the magnetic moments of the nucleons [the proton and neutron magnetic moments are $\mu_{p,n} = \frac{1}{2}(\mu_0 \pm \mu_1)$] is given by

$$\mathcal{L} = \frac{ie}{2M_N}F_{\mu\nu}(\mu_0\bar{N}[S^\mu, S^\nu]N + \mu_1\bar{N}[S^\mu, S^\nu]\tau^3_{\xi+}N), \tag{26}$$

for $\tau^a_{\xi\pm} = \frac{1}{2}(\xi^\dagger\tau^a\xi \pm \xi\tau^a\xi^\dagger)$.

There are other operators formally at this order which do not contribute to the polarizabilities at the order to which we work. There are kinetic operators and higher dimensional couplings of the baryons to the axial current whose coefficients are exactly fixed by the reparameterisation invariance of the baryon four-momentum [45,46]. These operators give the Z dependent pieces of the Compton amplitudes in Eq. (2). There are also additional operators with unconstrained coefficients such as $(\bar{\mathcal{B}}\mathcal{A}\cdot\mathcal{A}\mathcal{B})$ that contribute to the Compton amplitude at higher order. In two-flavor χPT there are two such operators, and in the SU(4|2) case there are ten [46].

The leading operators which contribute to the electromagnetic polarizabilities at tree level occur at $\mathcal{O}(Q^4)$ and

are given by the general form,

$$\frac{e^2 F_{\mu\rho} F^{\rho}_{\nu}}{\Lambda_\chi^3} (\bar{\mathcal{B}} \Gamma^{\mu\nu} \mathcal{Q}^2_{\xi\pm} \mathcal{B}),$$

(where the $\Gamma^{\mu\nu}$ are spin structures) while the leading tree-level contributions to the spin polarizabilities occur at $\mathcal{O}(Q^5)$. The complete set of such operators in the case of two-flavor χPT is given in Ref. [47]. Again there are significantly more such operators in QχPT and PQχPT. We do not explicitly show these operators, as they do not contribute at the order we are working and will not modify volume dependence until $\mathcal{O}(Q^6)$.

V. NUCLEON POLARIZABILITIES

Using the Lagrangian of the preceding section, we can calculate the amplitudes defined in Eq. (1) for Compton scattering from a nucleon (extensions to full octet and decuplet of baryons are straight-forward although the convergence of HBχPT with three-flavors is not clear). We work with a power counting such that

$$Q \sim e \sim \frac{|\vec{p}|}{\Lambda_\chi} \sim \frac{m_\pi}{\Lambda_\chi} \sim \frac{\omega}{\Lambda_\chi} \tag{27}$$

(it is also convenient to count Δ/Λ_χ as the same as Q as it is numerically similar at the masses relevant for current lattice calculations).[4] Below, we will also restrict ourselves to the low frequency limit $\omega \ll m_\pi$ in order to extract the polarizabilities from the Compton scattering amplitudes defined in Eqs. (1) and (2). For larger energies, the concept of polarizabilities breaks down and the target essentially becomes a dispersive medium. Working to order Q^3 in the chiral expansion, Compton scattering requires the calculation of the diagrams shown in Figs. 2–4 (and a corresponding set involving internal **44**-plet baryons). By definition, tree-level contributions from nucleon pole diagrams do not contribute to the polarizabilities; their contribution to the amplitudes are given explicitly in Eq. (2). For each polarizability $X = \alpha,\ \beta,\ \gamma_{1-4}$, it is convenient to separate the different contributions as

$$X = X^{\text{anomaly}} + X^{\Delta} + X^{\text{loop}}, \tag{28}$$

corresponding to the contributions from Figs. 2–4, respectively. We discuss these contributions in the following subsections. At order Q^3, all contributions are expressible in terms of a small set of LECs that contribute in many other processes and are thus reasonably well determined (at least in the χPT case). The total $\mathcal{O}(Q^3)$ loop contribution is finite, but loop contributions at higher orders are divergent; as discussed in the preceding section, the counter-terms specific to Compton scattering that absorb these divergences and the associated scale dependence enter at $\mathcal{O}(Q^4)$ for the electric and magnetic polarizabilities and $\mathcal{O}(Q^5)$ for the spin polarizabilities.

A. Volume independent contributions to polarizabilities

1. Anomalous contribution to $\gamma N \to \gamma N$: $\pi^0 \to \gamma\gamma$

The anomalous decay of flavor-neutral mesons to two photons [50,51] has important consequences in Compton scattering in nonforward directions. These contributions arise from the meson pole diagram shown in Fig. 2. Anomalous decays are well understood in χPT, entering through the Wess-Zumino-Witten (WZW) Lagrangian [42,43]. However, these effects have not been investigated in the quenched and partially-quenched theories and some interesting subtleties arise.

In SU(2) χPT, the one-pion, two-photon piece of the WZW Lagrangian, is given by

$$\mathcal{L}_{\pi^0\gamma\gamma} = -\frac{3e^2}{16\pi^2 f} \text{tr}[\phi \hat{\mathcal{Q}}^2] \epsilon^{\mu\nu\rho\sigma} F_{\mu\nu} F_{\rho\sigma}, \tag{29}$$

where

$$\phi = \begin{pmatrix} \frac{\pi^0}{\sqrt{2}} & \pi^+ \\ \pi^- & -\frac{\pi^0}{\sqrt{2}} \end{pmatrix}, \qquad \hat{\mathcal{Q}} = \begin{pmatrix} \frac{2}{3} & 0 \\ 0 & -\frac{1}{3} \end{pmatrix}. \tag{30}$$

This Lagrangian is completely determined as its coefficient can be fixed by directly matching to the perturbative QCD calculation of the relevant triangle diagram (the one loop calculation is exact [52], in accordance with Witten's geometric quantization condition [43]). At higher orders, additional anomalous operators appear [53] but they do not contribute to Compton scattering until $\mathcal{O}(Q^5)$.

It is well known that quenched and partially-quenched chiral perturbation theories generally have more complicated operator structure than in the case of QCD (e.g., one can not use Cayley-Hamilton identities [54]). Thus, in order to generalize Eq. (29) to the partially-quenched cases, we might imagine the extended $\pi^0 \to \gamma\gamma$ Lagrangian to be of the form

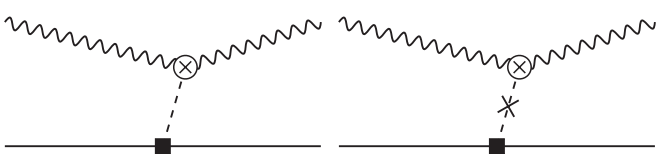

FIG. 2. Anomalous contributions to the polarizabilities. The crossed circle corresponds to the insertion of an operator from the Wess-Zumino-Witten Lagrangian, Eq. (32), and the crossed meson line corresponds to a hairpin interaction [76].

[4] Loop and pole [48] contributions with **44**-plet intermediate states must be included since Δ is a small-scale. Any Δ dependent terms analytic in m_π arising from the loop diagrams, and additional operators proportional to powers of Δ/Λ_χ can be resummed into the appropriate LECs of Δ independent operators (the LECs then depend on Δ) [46,49]. Keeping these contributions explicit is redundant as Δ can not be varied in a controlled manner.

$$\mathcal{L}^{PQ}_{\pi^0\gamma\gamma} \propto \epsilon^{\mu\nu\rho\sigma} F_{\mu\nu} F_{\rho\sigma} [a_1 \,\mathrm{str}[\Phi \mathcal{Q}^2] + a_2 \,\mathrm{str}[\Phi \mathcal{Q}]\,\mathrm{str}[\mathcal{Q}] + a_3 \,\mathrm{str}[\Phi]\,\mathrm{str}[\mathcal{Q}]^2 + a_4 \,\mathrm{str}[\Phi]\,\mathrm{str}[\mathcal{Q}^2]], \tag{31}$$

(in the quenched case only the first operator is nonvanishing, but a similar discussion applies). With the condition that in the QCD limit where the sea-quark and ghost-quark masses and charges are set equal to those of the valence quarks, matrix elements of Eq. (31) reproduce the matrix elements of Eq. (29). As discussed in Sec. IV, the singlet field, Φ_0 acquires a large mass from the strong $U(1)_A$ anomaly [39] and can be integrated out of the partially-quenched theory; consequently, the operators proportional to a_3 and a_4 can be ignored. Additionally, from the multiple supertrace structure, one can deduce that the operators

$$\mathrm{str}[\Phi \mathcal{Q}]\,\mathrm{str}[\mathcal{Q}], \qquad \mathrm{str}[\Phi]\,\mathrm{str}[\mathcal{Q}]^2, \qquad \mathrm{str}[\Phi]\,\mathrm{str}[\mathcal{Q}^2],$$

have at least two closed loops at the quark level. Following the arguments in Refs. [50–52], one can show that these operators do not correspond to anomalous quark-level processes. Moreover, the leading dependence of the underlying quark-level diagrams is proportional to the quark mass, and thus the coefficient of these operators must scale as, $a_{2,3,4} \sim m_q/\Lambda_\chi^2$. Although these operators contribute to $\eta_a \to \gamma\gamma$, they are not anomalous, and only contribute at higher orders in the chiral expansion. We can thus conclude that the only operator in the Lagrangian, Eq. (31), which contributes to the anomalous decay of the neutral mesons at leading order is $\mathrm{str}[\Phi \mathcal{Q}^2]$. The coefficient is easily determined by matching to either perturbative partially-quenched QCD or to the χPT expression in the QCD limit.[5] The appropriate Lagrangian is therefore

$$\mathcal{L}^{PQ}_{\pi^0\gamma\gamma} = -\frac{3e^2}{16\pi^2 f} \,\mathrm{str}[\Phi \mathcal{Q}^2] \epsilon^{\mu\nu\rho\sigma} F_{\mu\nu} F_{\rho\sigma}. \tag{32}$$

From the above Lagrangian, it is apparent that all of the flavor diagonal fields in Eq. (14), have anomalous couplings to two photons. Calculating the diagrams in Fig. 2 leads to the following anomalous contribution to Compton scattering on the proton[6] in partially-quenched χPT

$$T^{PQ,\mathrm{anomaly}}_{\mu\nu} = -i\epsilon_{\mu\nu\alpha\beta} k'^{\alpha} k^{\beta} r \cdot S \frac{24e^2}{(4\pi f)^2} \Bigg\{ 2g_A \Bigg[\left(q_u^2 - \frac{1}{2} q_j^2 - \frac{1}{2} q_l^2 \right) \frac{1}{r^2 - m_{uu}^2} + \frac{(q_j^2 - q_l^2)}{4} \frac{\Delta_{lj}^2}{(r^2 - m_{uu}^2)(r^2 - m_X^2)} \Bigg] + g_1 \Bigg[\left(q_u^2 - \frac{1}{2} q_j^2 - \frac{1}{2} q_l^2 \right) \frac{1}{r^2 - m_{uu}^2} - \left(\frac{1}{2} q_j^2 + \frac{1}{2} q_l^2 - q_d^2 \right) \frac{1}{r^2 - m_{dd}^2} - \frac{(q_j^2 - q_l^2)}{4} \frac{\Delta_{lj}^2}{(r^2 - m_X^2)} \left(\frac{1}{(r^2 - m_{uu}^2)} + \frac{1}{(r^2 - m_{dd}^2)} \right) \Bigg] \Bigg\}. \tag{33}$$

In the above expression, $r = q' - q$, is the momentum transfer to the nucleon and $\Delta_{lj}^2 = m_{ll}^2 - m_{jj}^2$ is a measure of the isospin breaking in the sea sector. In the sea isospin limit ($m_l \to m_j$), the double pole structure of the amplitude vanishes, and in the QCD limit all dependence on g_1 vanishes.

Expanding Eq. (33) in frequency and comparing with Eq. (1) leads to the following anomalous contributions to the polarizabilities:

$$\alpha^{\mathrm{anomaly}} = 0, \tag{34}$$

$$\beta^{\mathrm{anomaly}} = 0, \tag{35}$$

$$\gamma_1^{\mathrm{anomaly}} = -\frac{3e^2 G_{\mathrm{anom}}}{8\pi^3 f^2 m_\pi^2}, \tag{36}$$

$$\gamma_2^{\mathrm{anomaly}} = 0, \tag{37}$$

$$\gamma_3^{\mathrm{anomaly}} = \frac{3e^2 G_{\mathrm{anom}}}{16\pi^3 f^2 m_\pi^2}, \tag{38}$$

$$\gamma_4^{\mathrm{anomaly}} = -\frac{3e^2 G_{\mathrm{anom}}}{16\pi^3 f^2 m_\pi^2}, \tag{39}$$

where the coefficients, G_{anom}, are given in Table I for the different theories under consideration. These contributions vanish in the isoscalar combination of proton and neutron targets in the QCD limit.

2. Δ resonance contributions

The contributions to the amplitude from the Born terms involving the **44**-plet resonance (which contains the Δ-isobar), Fig. 3, are identical in χPT, PQχPT and QχPT as they are purely valence quark processes. They are given by

$$\alpha^{\Delta} = 0, \tag{40}$$

[5]We can thereby bypass the need to extend Witten's global quantization condition [43] to noncompact graded Lie groups.

[6]The anomalous contribution to neutron-Compton scattering is given by Eq. (33) with the interchange of $u \leftrightarrow d$.

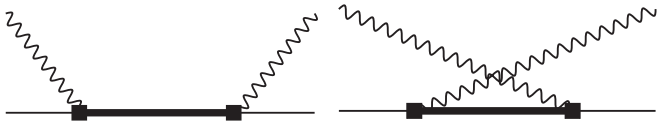

FIG. 3. Born diagrams involving internal **44**-plet states that give contribution to the polarizabilities.

$$\beta^{\Delta} = \mu_T^2 \frac{e^2(q_u - q_d)^2}{36\pi(2M_N)^2\Delta}, \tag{41}$$

$$\gamma_1^{\Delta} = 0, \tag{42}$$

$$\gamma_2^{\Delta} = -\mu_T^2 \frac{e^2(q_u - q_d)^2}{72\pi(2M_N)^2\Delta^2}, \tag{43}$$

$$\gamma_3^{\Delta} = 0, \tag{44}$$

$$\gamma_4^{\Delta} = \mu_T^2 \frac{e^2(q_u - q_d)^2}{72\pi(2M_N)^2\Delta^2}, \tag{45}$$

where μ_T is the magnetic dipole transition coupling of Eq. (23).

B. Infinite volume

The loop contributions to infinite volume chiral expansion of the polarizabilities in χPT are well known at order Q^3 [55–61] and at $\mathcal{O}(Q^4)$ [62–69] (at this order, the Δ-resonances have not been included as dynamical degrees of freedom, restricting the range of applicability to $m_\pi \ll \Delta$). Since the photon only couples to charged mesons, the results in the quenched and partially-quenched theories are similar to those in χPT. In particular, no quenched or partially-quenched sicknesses (double pole contributions from neutral meson propagators) enter expression for the loop diagrams. In general, the quenched power counting presents differences for electromagnetic observables [33,36,44,70], however no new contributions appear at the order we work.

Using the effective couplings G_B, G'_B, G_T and G'_T given in Table I, we find that the loop contributions to the polarizabilities are

$$\alpha^{\rm loop} = \frac{e^2}{4\pi f^2}\left[\frac{5G_B}{192\pi}\frac{1}{m_\pi} + \frac{5G'_B}{192\pi}\frac{1}{m_{uj}} + \frac{G_T}{72\pi^2}F_\alpha(m_\pi,\Delta) + \frac{G'_T}{72\pi^2}F_\alpha(m_{uj},\Delta)\right], \tag{46}$$

$$\beta^{\rm loop} = \frac{e^2}{4\pi f^2}\left[\frac{G_B}{384\pi}\frac{1}{m_\pi} + \frac{G'_B}{384\pi}\frac{1}{m_{uj}} + \frac{G_T}{72\pi^2}F_\beta(m_\pi,\Delta) + \frac{G'_T}{72\pi^2}F_\beta(m_{uj},\Delta)\right], \tag{47}$$

$$\gamma_1^{\rm loop} = \frac{e^2}{4\pi f^2}\left[\frac{G_B}{48\pi^2}\frac{1}{m_\pi^2} + \frac{G'_B}{48\pi^2}\frac{1}{m_{uj}^2} + \frac{G_T}{72\pi^2}F_{\gamma_1}(m_\pi,\Delta) + \frac{G'_T}{72\pi^2}F_{\gamma_1}(m_{uj},\Delta)\right], \tag{48}$$

$$\gamma_2^{\rm loop} = \frac{e^2}{4\pi f^2}\left[\frac{G_B}{96\pi^2}\frac{1}{m_\pi^2} + \frac{G'_B}{96\pi^2}\frac{1}{m_{uj}^2} + \frac{G_T}{72\pi^2}F_{\gamma_2}(m_\pi,\Delta) + \frac{G'_T}{72\pi^2}F_{\gamma_2}(m_{uj},\Delta)\right], \tag{49}$$

$$\gamma_3^{\rm loop} = \frac{e^2}{4\pi f^2}\left[\frac{G_B}{192\pi^2}\frac{1}{m_\pi^2} + \frac{G'_B}{192\pi^2}\frac{1}{m_{uj}^2} + \frac{G_T}{144\pi^2}F_{\gamma_3}(m_\pi,\Delta) + \frac{G'_T}{144\pi^2}F_{\gamma_3}(m_{uj},\Delta)\right], \tag{50}$$

$$\gamma_4^{\rm loop} = -\frac{e^2}{4\pi f^2}\left[\frac{G_B}{192\pi^2}\frac{1}{m_\pi^2} + \frac{G'_B}{192\pi^2}\frac{1}{m_{uj}^2} + \frac{G_T}{144\pi^2}F_{\gamma_4}(m_\pi,\Delta) + \frac{G'_T}{144\pi^2}F_{\gamma_4}(m_{uj},\Delta)\right], \tag{51}$$

where

TABLE I. Effective couplings for the various contributions to the polarizabilities.

	QCD	QQCD	PQQCD
$G_{\rm anom}$	$g_A(2Z-1)(q_u^2 - q_d^2)$	$2g_A(Zq_u^2 + (1-Z)q_d^2) + g_1(q_d^2 + q_u^2)$	$g_A[2(Zq_u^2 + (1-Z)q_d^2) - q_j^2 - q_l^2] + g_1(q_d^2 - q_j^2 - q_l^2 + q_u^2)$
G_B	$4g_A^2(q_d - q_u)^2$	$\frac{1}{3}(4g_A^2 - 4g_Ag_1 - 5g_1^2)(q_d - q_u)^2$	$-\frac{1}{3}(5g_1^2 + 4g_Ag_1 - 4g_A^2)(q_d - q_u)^2$
G'_B	0	0	$\frac{1}{3}[(6q_d^2 - 6(q_j+q_l)q_d + 5q_j^2 + 5q_l^2 + 4q_u^2 - 4q_jq_u - 4q_lq_u)g_1^2 + 4g_A(q_j^2 - 2q_uq_j + q_l^2 + 2q_u^2 - 2q_lq_u)g_1 + 8g_A^2(q_j^2 - 2q_uq_j + q_l^2 + 2q_u^2 - 2q_lq_u)]$
G_T	$\frac{4}{3}g_{\Delta N}^2(q_d - q_u)^2$	$\frac{5}{6}g_{\Delta N}^2(q_d - q_u)^2$	$\frac{5}{6}g_{\Delta N}^2(q_d - q_u)^2$
G'_T	0	0	$\frac{1}{6}g_{\Delta N}^2(4q_d^2 - 4(q_j+q_l)q_d + 3q_j^2 + 3q_l^2 + 2q_u^2 - 2q_jq_u - 2q_lq_u)$

$$F_\alpha(m,\Delta) = \frac{9\Delta}{\Delta^2 - m^2} - \frac{\Delta^2 - 10m^2}{2(\Delta^2 - m^2)^{3/2}} \times \ln\left[\frac{\Delta - \sqrt{\Delta^2 - m^2 + i\epsilon}}{\Delta + \sqrt{\Delta^2 - m^2 + i\epsilon}}\right], \quad (52)$$

$$F_\beta(m,\Delta) = -\frac{1}{2(\Delta^2 - m^2)^{1/2}} \ln\left[\frac{\Delta - \sqrt{\Delta^2 - m^2 + i\epsilon}}{\Delta + \sqrt{\Delta^2 - m^2 + i\epsilon}}\right], \quad (53)$$

$$F_{\gamma_1}(m,\Delta) = -\frac{\Delta^2 + 2m^2}{(\Delta^2 - m^2)^2} - \frac{3\Delta m^2}{2(\Delta^2 - m^2)^{5/2}} \times \ln\left[\frac{\Delta - \sqrt{\Delta^2 - m^2 + i\epsilon}}{\Delta + \sqrt{\Delta^2 - m^2 + i\epsilon}}\right], \quad (54)$$

$$F_{\gamma_2}(m,\Delta) = F_{\gamma_3}(m,\Delta) = F_{\gamma_4}(m,\Delta) = \frac{1}{\Delta^2 - m^2} + \frac{\Delta}{2(\Delta^2 - m^2)^{3/2}} \times \ln\left[\frac{\Delta - \sqrt{\Delta^2 - m^2 + i\epsilon}}{\Delta + \sqrt{\Delta^2 - m^2 + i\epsilon}}\right]. \quad (55)$$

Here we have used dimensional regularization, however the results are finite and hence independent of the regulator without the addition of counterterms. These loop contributions vanish at zero photon frequency, preserving the Thompson limit. They are identical for both proton and neutron targets, though isospin breaking effects from loops enter at $\mathcal{O}(Q^4)$ in the expansion. In the χPT case, these results reproduce those of Refs. [58,59].

C. Finite volume

In momentum space, the finite volume of a lattice simulation restricts the available momentum modes and consequently the results differ from their infinite volume values. These long-distance effects can be accounted for in the low-energy effective theory. Here we shall consider a hyper-cubic box of dimensions $L^3 \times T$ with $T \gg L$. Imposing periodic boundary conditions on mesonic fields leads to quantized momenta $k = (k_0, \vec{k})$, $\vec{k} = \frac{2\pi}{L}\vec{j} = \frac{2\pi}{L} \times (j_1, j_2, j_3)$ with $j_i \in \mathbb{Z}$, but k_0 treated as continuous. On such a finite volume, spatial momentum integrals are replaced by sums over the available momentum modes. This leads to modifications of the infinite volume results presented in the previous section; the various functions arising from loop integrals are replaced by their finite volume (FV) counterparts. In a system where $m_\pi L \gg 1$, the power counting of the infinite volume low-energy effective theory remains valid and finite volume effects are predominantly from Goldstone mesons propagating to large distances where they are sensitive to boundary conditions and can even "wrap around the world". Smaller volumes in which $m_\pi L \sim 1$ are discussed in Appendix B. Since the lowest momentum mode of the Goldstone propagator is $\sim \exp(-m_\pi L)$ in position space, finite volume effects will behave as a polynomial in $1/L$ times this exponential if no multiparticle thresholds are reached in the loop (as is the case in these calculations provided the photon energy is small enough, $\omega \lesssim m_\pi$).

Repeating the calculation of the loop diagrams using finite volume sums rather than integrals leads to the following expressions for the loop contributions to the polarizabilities:

$$\alpha^{\text{loop}}(L) = \frac{e^2}{1152\pi f^2}\int_0^\infty d\lambda[3G_B\mathcal{F}_\alpha(\mathcal{M}_{uu}) + 3G'_B\mathcal{F}_\alpha(\mathcal{M}_{uj}) + 8G_T\mathcal{F}_\alpha(\mathcal{M}^\Delta_{uu}) + 8G'_T\mathcal{F}_\alpha(\mathcal{M}^\Delta_{uj})], \quad (56)$$

$$\beta^{\text{loop}}(L) = \frac{e^2}{1152\pi f^2}\int_0^\infty d\lambda[3G_B\mathcal{F}_\beta(\mathcal{M}_{uu}) + 3G'_B\mathcal{F}_\beta(\mathcal{M}_{uj}) + 8G_T\mathcal{F}_\beta(\mathcal{M}^\Delta_{uu}) + 8G'_T\mathcal{F}_\beta(\mathcal{M}^\Delta_{uj})], \quad (57)$$

$$\gamma_1^{\text{loop}}(L) = \frac{7e^2}{576\pi f^2}\int_0^\infty d\lambda[3G_B\mathcal{F}_{\gamma_1}(\mathcal{M}_{uu}) + 3G'_B\mathcal{F}_{\gamma_1}(\mathcal{M}_{uj}) - 4G_T\mathcal{F}_{\gamma_1}(\mathcal{M}^\Delta_{uu}) - 4G'_T\mathcal{F}_{\gamma_1}(\mathcal{M}^\Delta_{uj})], \quad (58)$$

$$\gamma_2^{\text{loop}}(L) = \frac{7e^2}{64\pi f^2}\int_0^\infty d\lambda[3G_B\mathcal{F}_{\gamma_2}(\mathcal{M}_{uu}) + 3G'_B\mathcal{F}_{\gamma_2}(\mathcal{M}_{uj}) - 4G_T\mathcal{F}_{\gamma_2}(\mathcal{M}^\Delta_{uu}) - 4G'_T\mathcal{F}_{\gamma_2}(\mathcal{M}^\Delta_{uj})], \quad (59)$$

$$\gamma_3^{\text{loop}}(L) = \frac{7e^2}{1152\pi f^2}\int_0^\infty d\lambda[3G_B\mathcal{F}_{\gamma_3}(\mathcal{M}_{uu}) + 3G'_B\mathcal{F}_{\gamma_3}(\mathcal{M}_{uj}) - 4G_T\mathcal{F}_{\gamma_3}(\mathcal{M}^\Delta_{uu}) - 4G'_T\mathcal{F}_{\gamma_3}(\mathcal{M}^\Delta_{uj})], \quad (60)$$

$$\gamma_4^{\text{loop}}(L) = -\gamma_3^{\text{loop}}(L), \quad (61)$$

where $\mathcal{M}_{ab} = \sqrt{m_{ab}^2 + \lambda^2}$ and $\mathcal{M}^\Delta_{ab} = \sqrt{m_{ab}^2 + 2\lambda\Delta + \lambda^2}$ and

$$\mathcal{F}_\alpha(m) = 180\lambda^2\mathcal{I}_{7/2}(m) + 190\mathcal{J}_{7/2}(m) - 280\lambda^2\mathcal{J}_{9/2}(m) - 455\mathcal{K}_{9/2}(m) + 315\lambda^2\mathcal{K}_{11/2}(m) + 252\mathcal{L}_{11/2}(m), \quad (62)$$

$$\mathcal{F}_\beta(m) = 60\mathcal{J}_{7/2}(m) - 224\mathcal{K}_{9/2}(m) + 189\mathcal{L}_{11/2}(m), \quad (63)$$

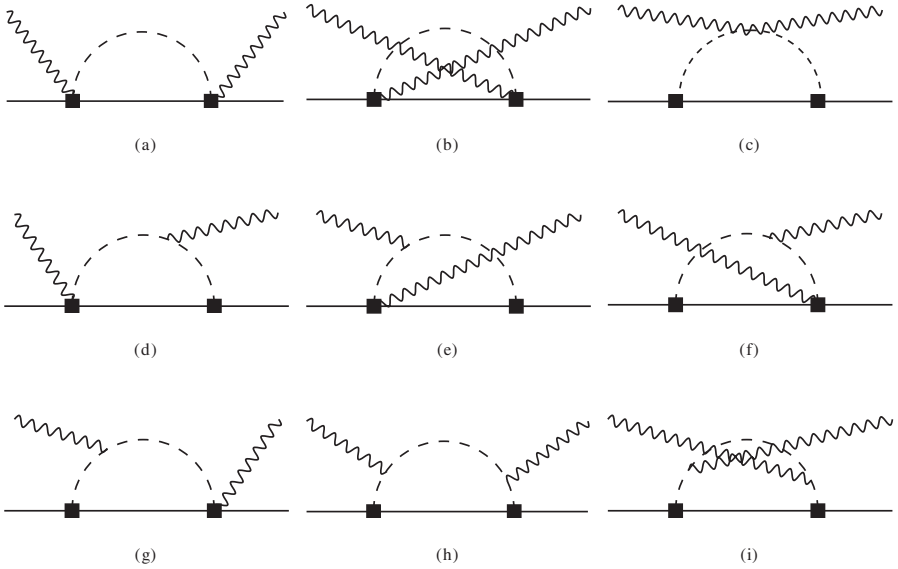

FIG. 4. Diagrams contributing to nucleon polarizabilities at order Q^3. The solid and dashed lines denote nucleons, and pions, respectively. Additionally, our results include a similar set of diagrams in which the internal **70**-plet propagator is replaced by a **44**-plet resonance.

$$\mathcal{F}_{\gamma_1}(m) = 30\lambda^3 \mathcal{I}_{9/2}(m) + 10\lambda \mathcal{J}_{9/2}(m) - 45\lambda^3 \mathcal{J}_{11/2}(m) - 18\lambda \mathcal{K}_{11/2}(m), \tag{64}$$

$$\mathcal{F}_{\gamma_2}(m) = \lambda \mathcal{K}_{11/2}(m), \tag{65}$$

$$\mathcal{F}_{\gamma_3}(m) = 10\lambda \mathcal{J}_{9/2}(m) - 9\lambda \mathcal{K}_{11/2}(m), \tag{66}$$

and the finite volume sums $\mathcal{I}_\beta(m), \ldots, \mathcal{L}_\beta(m)$ are defined in Appendix C. These expressions reduce to the results of Eqs. (46)–(51) above in the infinite volume limit.

To illustrate these effects, Figs. 5 and 6 show the volume dependence of the various polarizabilities in the proton and the neutron, respectively. Here we have specialized to QCD, setting $q_u = 2/3$, $q_d = -1/3$, $g_A = 1.25$, $|g_{N\Delta}| = 1.5$, $\mu_T = 10.9$, $f = 0.132$ GeV, $M_N = 0.938$ GeV and $\Delta = 0.3$ GeV.[7] In each plot we show results for the ratio

$$\Delta X(L) = \frac{X(L) - X(\infty)}{X(\infty)}, \tag{67}$$

for the six polarizabilities at three different pion masses, $m_\pi = 0.25, 0.35, 0.50$ GeV. The overall magnitude of these shifts varies considerably; generally volume effects are at the level of 5%–10% for $m_\pi = 0.25$ GeV and smaller for larger masses. Larger effects are seen in a number of the spin polarizabilities but there are as yet no lattice calculations of these quantities. The magnetic polarizability has a particularly small volume dependence which can be understood from the large decouplet resonance contribution that is independent of the volume.

The above expressions also allow us to calculate the finite volume effects in the quenched data on the various polarizabilities calculated in Refs. [7,8]. The quenched expressions involve a number of undetermined LECs (quenched g_A, g_1, $g_{N\Delta}$ and μ_T are unrelated to their PQχPT/χPT values), so we can only estimate the volume effects. To do so, we choose $q_u = 2/3$, $q_d = -1/3$, $g_A = 1.25$, $g_1 = 1$, $|g_{N\Delta}| = 1.5$, $\mu_T = 5.85$, $f = 0.132$ GeV, $M_N = 0.938$ GeV and $\Delta = 0.3$ GeV and take the pion masses corresponding to the lightest used in these lattice calculations, $m_\pi \sim 0.5$ GeV (we ignore the issue of the convergence of χPT at such masses). The results for the volume dependence of the various polarizabilities of the proton and neutron are shown in Figs. 7 and 8. In each plot, the shaded region corresponds to reasonable variation of the unknown couplings, $-1 < g_1 < 1$, $0.8 < |g_{N\Delta}| < 2$ and $2.8 < |\mu_T| < 8.5$. From these figures, we see that the calculations on a $(2.4\text{ fm})^3$ lattice with $m_\pi = 0.5$ GeV may differ from their infinite volume values by 5–10% in the case of the electric polarizability and a few percent for the magnetic and spin polarizabilities.

An interesting effect that arises at finite volume is that the Thompson limit and other Born terms in the frequency expansion of the scattering amplitude (terms in Eq. (2) that are not polarizabilities) receive finite volume contributions from the loop diagrams in Fig. 4 that vanish exponentially as the volume is increased. As an example, the amplitude for Thomson-limit (zero frequency) scattering on the neutron (which is identically zero at infinite volume) is shown in Fig. 9. This result is somewhat counter-intuitive, but arises from the effects of the periodic boundary conditions

[7]The value of μ_T is chosen to correspond to that found in analysis of Ref. [59] ($\mu_T = 2\sqrt{2}b_1$ of that reference). In principle this LEC can be determined from an analysis of lattice polarizabilities or $N - \Delta$ transition matrix elements.

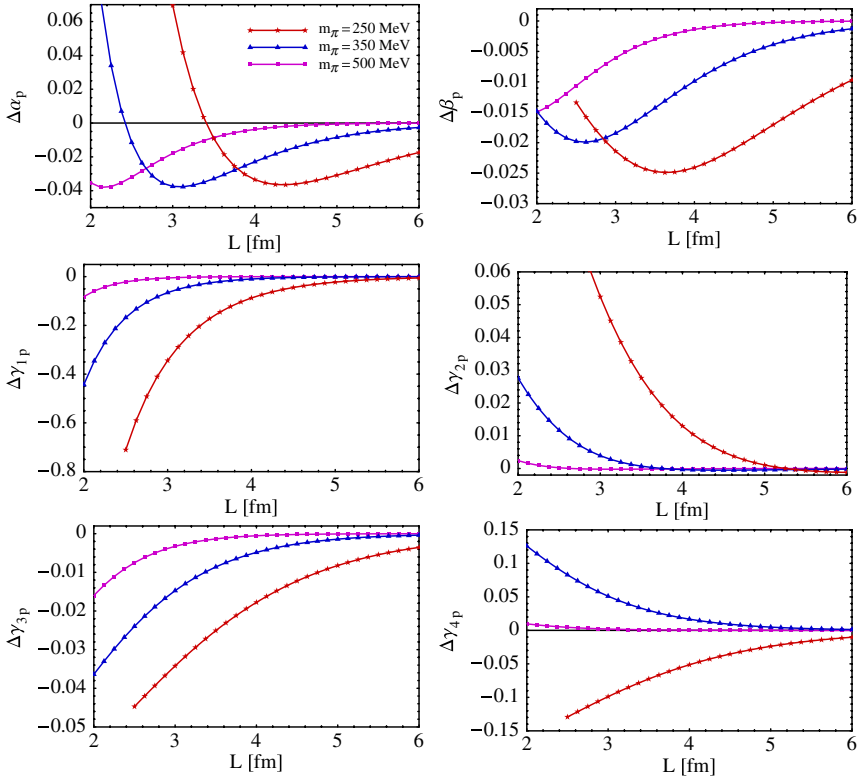

FIG. 5 (color online). Volume dependence of the proton polarizabilities. Here we show the ratio of the difference of the finite and infinite volume results to the infinite volume results for three values of the pion mass using the parameters described in the text. The curves terminate at $m_\pi L = 3$.

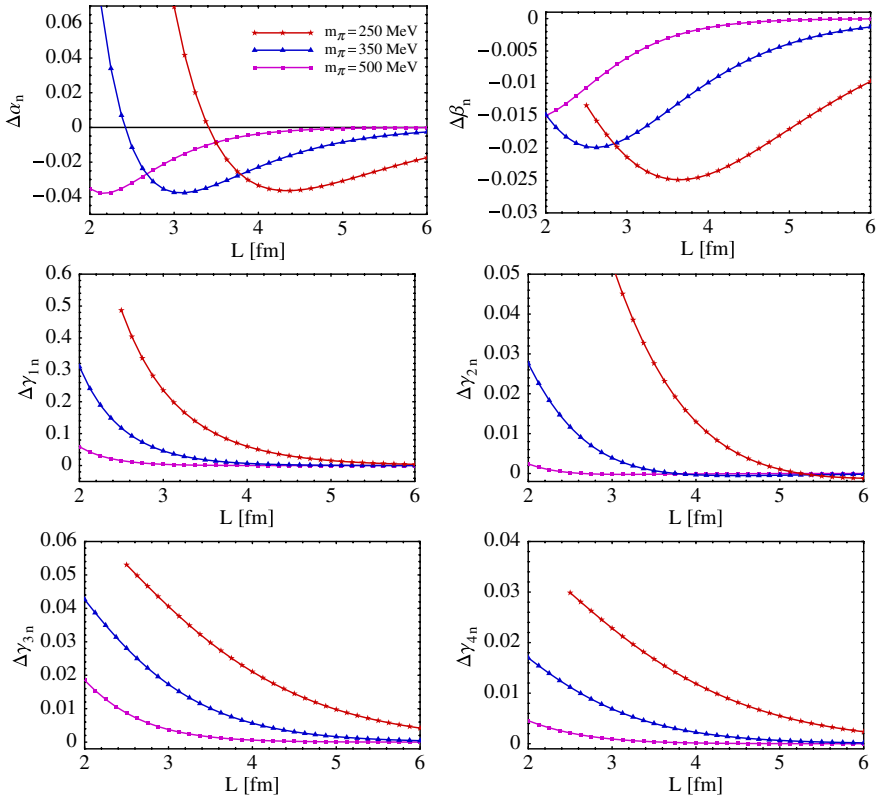

FIG. 6 (color online). Volume dependence of the neutron polarizabilities. The various curves are as in Fig. 5.

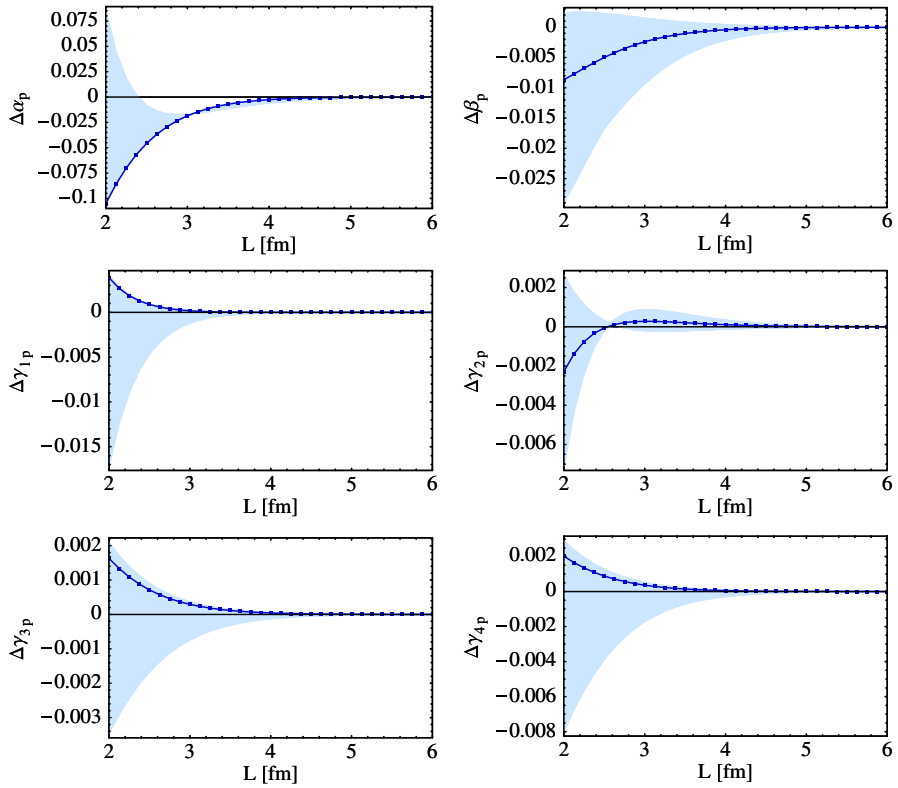

FIG. 7 (color online). Volume dependence of the proton polarizabilities in quenched QCD at the lightest quark mass used in the lattice calculations of Refs. [7,8]. The central curves and shaded region correspond to the parameters quoted in the text.

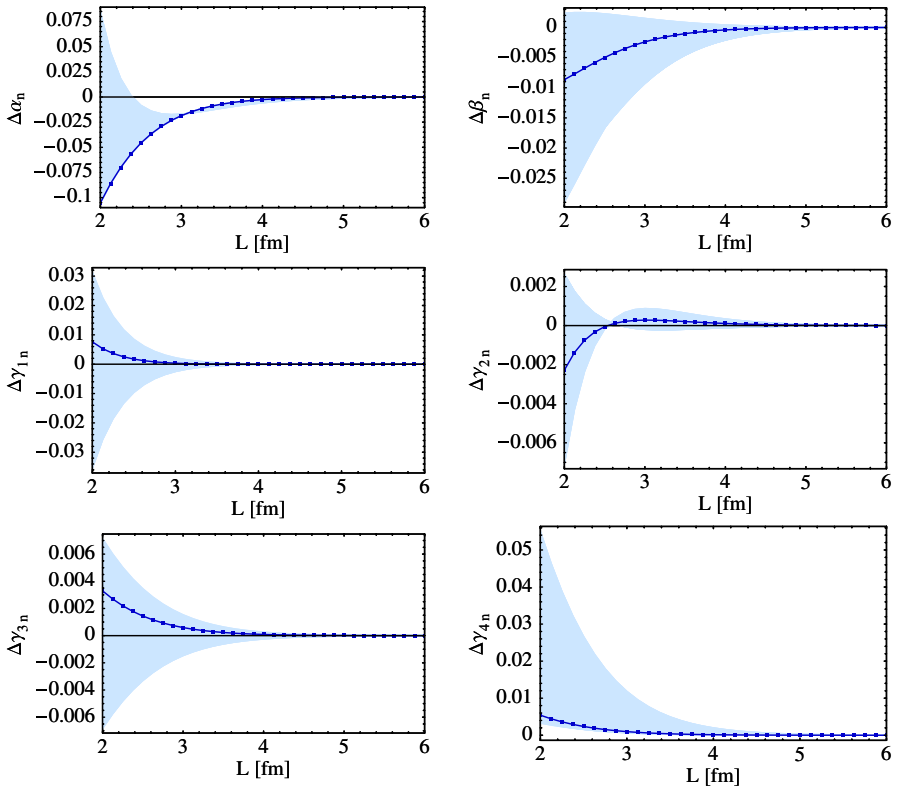

FIG. 8 (color online). As in Fig. 7, but for the neutron.

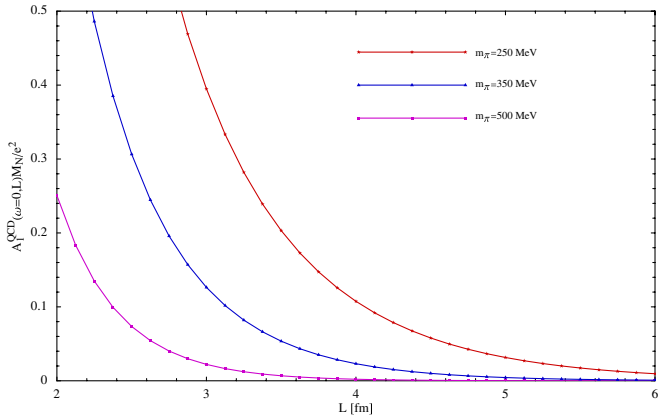

FIG. 9 (color online). Volume dependence of the Thompson limit of photon neutron scattering. Notice the infinite volume limit is zero.

on the long range charge distribution of the hadron. It does not imply the nonconservation of charge.

The results presented here all assume that the higher-order terms in the Q expansion provide small contributions to the volume dependence of the polarizabilities. This may or may not be the case as diagrams that are formally of higher-order in the infinite volume χPT power-counting can have volume effects that are enhanced over those at lower infinite volume order (see Ref. [41] for a detailed discussion). Such issues may be particularly relevant for the polarizabilities where the convergence of the chiral expansion is tenuous. In this regard, studying the FV behavior of the lattice results may in fact be a useful diagnostic tool with which to determine if or why the convergence is poor.

VI. CONCLUSION

We have investigated Compton scattering from spin-half targets from the point of view of lattice QCD. We first discussed how external field methods can be used to probe all six polarizabilities of real Compton scattering for both charged and uncharged targets. Such calculations will tell us a lot about the low-energy QCD structure of hadrons and will be of much use in phenomenological studies requiring the full set of polarizabilities as only certain linear combinations are available from current experiments [1,2]. The techniques discussed here also allow us to extract other electric properties of charged particles using external fields including the electric dipole moment of the proton and the quadrupole moment of the deuteron.

Our second major focus was on the effects of the finite volume used in lattice calculations on the polarizabilities. Since polarizabilities are infrared-sensitive observables (they scale as inverse powers of the pion mass near the chiral limit), the are expected to have strong volume dependence. This is indeed borne out in the explicit calculations presented here. In QCD, we generically find that the polarizabilities experience volume shifts of 5–10% from the infinite volume values for lattice volumes $\sim(2.4\ \mathrm{fm})^3$ and pions of mass 0.25 GeV. The electric and first spin polarizabilities are particularly sensitive. In the case of quenched QCD (relevant to the only existing lattice data), we find significant effects even at pion masses $\sim$0.5 GeV. Future lattice studies of the polarizabilities should take these effects into account in order to present physically relevant results.

As extensions of this work, one can also consider the generalized polarizabilities, higher-order polarizabilities and parity violating polarizabilities (see Ref. [71]) all of which can be extracted from appropriate lattice calculations similar to those detailed in Sec. III. Such information would lead to a further-improved understanding of the low-energy structure of the hadrons and prove very useful in directing the next generation of precision Compton scattering experiments. The lattice provides a novel opportunity to study the neutron polarizabilities directly instead of from nuclear targets and extending the lattice methods of Sec. III to the deuteron (along similar lines to those discussed in Ref. [72]) will also prove useful for comparison to experiment.

ACKNOWLEDGMENTS

We express our gratitude to C.-J. D. Lin, D. O'Connell, D. R. Phillips, M. J. Savage, S. R. Sharpe, R. M. Woloshyn, and R. D. Young for many helpful discussions. This work is supported by the US Department of Energy under Contract Nos. DE-FG02-97ER41014 (W. D. and A. W-L.) and DE-FG02-05ER41368-0 (B. C. T.).

APPENDIX A: QUENCHED CHIRAL LAGRANGIAN

In this Appendix, we display the relevant pieces of the quenched chiral Lagrangian in the meson and baryon sectors and note particular pathologies of the quenched theory. In a quenched two-flavor theory, we have valence (u, d) and ghost $(\tilde{u}, \tilde{d})$ quarks with masses contained in the matrix

$$\bar{m}_Q = \mathrm{diag}(m_u, m_d, m_{\tilde{u}}, m_{\tilde{d}}), \tag{A1}$$

where $m_{\tilde{u},\tilde{d}} = m_{u,d}$ to maintain the exact cancellation from the path-integral determinants arising from the valence and ghost-quark sectors. The corresponding low-energy meson dynamics are described by the QχPT Lagrangian. At leading order, the form of this Lagrangian is the same as in Eq. (12) where the pseudo-Goldstone mesons are embedded nonlinearly in Σ with the matrix Φ now given by

$$\Phi = \begin{pmatrix} M & \chi^\dagger \\ \chi & \tilde{M} \end{pmatrix}, \tag{A2}$$

where

$$M = \begin{pmatrix} \eta_u & \pi^+ \\ \pi^- & \eta_d \end{pmatrix}, \qquad \tilde{M} = \begin{pmatrix} \tilde{\eta}_u & \tilde{\pi}^+ \\ \tilde{\pi}^- & \tilde{\eta}_d \end{pmatrix}, \qquad \chi = \begin{pmatrix} \chi_{\eta_u} & \chi_{\pi^+} \\ \chi_{\pi^-} & \chi_{\eta_d} \end{pmatrix}. \tag{A3}$$

The matrix M contains the usual valence-valence mesons, while mesons in $\tilde{M}$ are composed of ghost quarks and antiquarks, and finally those in χ of ghost–valence quark–antiquark pairs. Unlike the partially-quenched theory, there is no strong $U(1)_A$ anomaly, and the flavor-singlet field, $\Phi_0 = \mathrm{str}[\Phi]/\sqrt{2}$ (along with its couplings m_0 and α_Φ), must be retained in the theory. For the electromagnetic and spin polarizabilities in QQCD, no loop contributions from the singlet are needed to the order we work as flavor-neutral mesons are not present in loop diagrams at this order. Despite flavor-neutral mesons being absent in loop graphs, the anomalous tree-level term couples the quenched singlet to the nucleon. Cancellations, however, lead to final results that are independent of m_0 and α_Φ.

For the quenched electric charge matrix of the valence and ghost quarks, we choose

$$\hat{\mathcal{Q}} = \mathrm{diag}(q_u, q_d, q_u, q_d). \tag{A4}$$

Notice the peculiarity that $\mathrm{str}\,\hat{\mathcal{Q}} = 0$ is unavoidable in the quenched theory. In the quenched theory, there are anomalous decays of flavor-neutral mesons into two photons. In terms of SU(2|2) QQCD quark fields, contributions to the anomaly from the valence and ghost sectors come weighted with squares of the quark charges, and we are thus not restricted to only the flavor-singlet current (as is the case for the strong $U(1)_A$ anomaly). The relevant term of the anomalous quenched chiral Lagrangian is the same as has been detailed above in Sec. VA 1.

In SU(2|2) HBχPT, the nucleons (those composed of three valence quarks) enter as part of a **20**-dimensional representation described by a three index flavor-tensor, $\mathcal{B}$. The quenched Δ-isobar is contained in the totally symmetric three index flavor-tensor $\mathcal{T}^\mu$ transforming in the **12**-dimensional representation of SU(2|2). The leading-order Lagrangian describing these baryons and their interactions with Goldstone mesons is

$$\begin{aligned} \mathcal{L}^{(0)}_{BQ} &= i(\bar{\mathcal{B}} v\cdot\mathcal{D}\mathcal{B}) + 2\alpha(\bar{\mathcal{B}} S^\mu \mathcal{B}\mathcal{A}_\mu) \\ &\quad + 2\beta(\bar{\mathcal{B}} S^\mu \mathcal{A}_\mu \mathcal{B}) + 2\gamma(\bar{\mathcal{B}} S^\mu \mathcal{B})\,\mathrm{str}\mathcal{A}_\mu \\ &\quad - i(\bar{\mathcal{T}}^\mu v\cdot\mathcal{D}\mathcal{T}_\mu) + \Delta(\overline{\mathcal{T}}^\mu \mathcal{T}_\mu) \\ &\quad + 2\mathcal{H}(\overline{\mathcal{T}}^\nu S^\mu \mathcal{A}_\mu \mathcal{T}_\nu) + 2\gamma'(\overline{\mathcal{T}}^\nu S^\mu \mathcal{T}_\nu)\,\mathrm{str}\mathcal{A}_\mu \\ &\quad + \sqrt{\frac{3}{2}}\mathcal{C}[(\overline{\mathcal{T}}^\nu \mathcal{A}_\nu \mathcal{B}) + (\bar{\mathcal{B}}\mathcal{A}_\nu \mathcal{T}^\nu)]. \end{aligned} \tag{A5}$$

In contrast to partially-quenched and unquenched chiral perturbation theory, there are two additional axial couplings γ and γ' due to the presence of the flavor-singlet field. One should keep in mind that although we use the same notation for simplicity, all of the coefficients in the quenched Lagrangian have distinct numerical values from those of the partially-quenched Lagrangian. In the large N_c limit, the coefficients of the two theories are related [73].

Again the photon is minimally coupled in the above Lagrangian with fixed coefficients. At the next order in the expansion, the relevant terms that appear are

$$\begin{aligned} \mathcal{L}^{(1)}_{BQ} &= \frac{ie}{2M_N} F_{\mu\nu}[\mu_\alpha(\bar{\mathcal{B}}[S^\mu, S^\nu]\mathcal{B}\mathcal{Q}_{\xi+}) \\ &\quad + \mu_\beta(\bar{\mathcal{B}}[S^\mu, S^\nu]\mathcal{Q}_{\xi+}\mathcal{B})] \\ &\quad + \sqrt{\frac{3}{2}}\mu_T \frac{ie}{2M_N} F_{\mu\nu}[(\bar{\mathcal{B}} S^\mu \mathcal{Q}_{\xi+}\mathcal{T}^\nu) \\ &\quad + (\bar{\mathcal{T}}^\mu S^\nu \mathcal{Q}_{\xi+}\mathcal{B})]. \end{aligned} \tag{A6}$$

The PQχPT term with coefficient μ_γ is absent in the quenched theory. This only affects the Born terms of the Compton amplitude, which are essentially unknown because they depend on the quenched magnetic moment. Finally, the leading two-photon operators that give completely local contributions to the Compton scattering tensor appear in quenched chiral perturbation theory in essentially the same form as PQχPT. However, there are fewer operators per spin structure compared to the partially-quenched case because of the supertracelessness of the electric charge matrix. Our computation is unchanged since these terms do not contribute at the order we work.

APPENDIX B: COMPTON SCATTERING IN SMALL VOLUMES

In this appendix, we discuss the volume dependence of the polarizabilities on asymmetric lattices in which the spatial dimensions are small but the temporal direction remains large: $m_\pi L \ll 1$ but $L^3 T m_q \langle\bar{q}q\rangle \gg 1$.[8] In this ϵ'-regime [75], $m_\pi \sim \epsilon'^2$ and $L \sim \epsilon'^{-1}$ (where ϵ' is the small expansion parameter) so Goldstone boson zero modes (modes with $\vec{q} = 0$) are enhanced, but remain perturbative. Thus, the power counting of loop diagrams involving zero-modes is modified. In Compton scattering at finite volume, the photon momenta provide additional scales whose power-counting must be specified. The spatial components of the incoming and outgoing photon momenta are quantized as $\vec{q}^{(\prime)} = \frac{2\pi}{L}\vec{n}_{q^{(\prime)}}$ (where $\vec{n}_{q^{(\prime)}}$ are integer 3-tuples) and consequently scale as $\mathcal{O}(\epsilon')$. For real Compton scattering, $q_0^{(\prime)2} = |\vec{q}^{(\prime)}|^2$, implying that the frequency ω is either zero or also $\mathcal{O}(\epsilon')$, parametrically larger than the pion mass, $\omega/m_\pi \gg 1$. This introduces an intrin-

[8]The calculation of the volume dependence of the polarizabilities in the ϵ-regime [74] (where $m_\pi L \sim m_\pi T \sim 1$ and $L^3 T m_q \langle\bar{q}q\rangle \sim 1$ and zero-modes become nonperturbative) is beyond the scope of this work.

sic difficulty in defining polarizabilities for realistic pion masses in small volumes, as they arise from an expansion around the zero frequency limit. Thus our discussion is restricted to the full amplitudes $A_i(\omega, \theta)$ in Eq. (1). This is not an issue in larger volumes (Sec. V C above) as the quantization of momenta is fine-grained on the scale of m_π. In (doubly) virtual Compton scattering, the on-shell condition is relaxed and one can again consider nonzero energies comparable to or smaller than the pion mass.

In the ϵ'-regime, the loop diagrams in Fig. 4 generically contribute at order ϵ'^3 for nonzero modes (we count $e \sim \epsilon'$). However, diagrams 3(a) and 3(b) contain nonderivative couplings and zero-modes provide a further enhanced contribution, $\sim\epsilon'$. Although the remaining diagrams in Fig. 4 contain derivatively coupled pions, the nonzero momentum insertions allow the energy integral to be performed with a pole $k_0 \sim m_\pi \sim \epsilon'^2$, leading to a putative enhancement. However, transversality of the Compton amplitude causes these enhanced contributions to vanish. Thus $A_1(\omega = 0)$ receives contributions at $\mathcal{O}(\epsilon')$ and A_3 at $\mathcal{O}(\epsilon'^2)$ and these amplitudes will exhibit enhanced volume dependence for lattice calculations in the ϵ'-regime. This dependence is given by

$$A_1(\omega, \theta) = \frac{e^2 G_B}{4 m_\pi^2 L^3} + \frac{2 e^2 G_T}{3 m_\pi L^3} \frac{1}{m_\pi + \Delta} + \mathcal{O}(\epsilon'^3), \quad \text{(B1)}$$

$$A_3(\omega, \theta) = \frac{e^2 G_B}{4 m_\pi L^3} \frac{\omega}{m_\pi^2 - \omega^2} - \frac{e^2 G_T}{3 m_\pi L^3} \frac{\omega}{(m_\pi + \Delta)^2 - \omega^2} + \mathcal{O}(\epsilon'^3). \quad \text{(B2)}$$

Since m_π is necessarily smaller than any nonzero value of ω in the small volume regimes, pions can go on-shell in the loop diagrams of Fig. 4. Consequently the power-law dependence on volume seen in Eqs. (B1) and (B2) is not unexpected. The other amplitudes have contributions from the diagrams in Fig. 4 starting at $\mathcal{O}(\epsilon'^3)$. At this order additional diagrams such as those arising from tadpole dressings of the vertices in Fig. 4(a) and 4(b) also contribute and the full results are left to future work.

APPENDIX C: FINITE VOLUME FUNCTIONS

The sums required in the evaluation of the polarizabilities at finite volume are ($\vec{k} = \frac{2\pi\vec{n}}{L}$, with $\vec{n}$ a triplet of integers)

$$\mathcal{I}_\beta(M) = \frac{1}{L^3} \sum_{\vec{k}} \frac{1}{[|\vec{k}|^2 + M^2]^\beta}, \quad \text{(C1)}$$

$$\mathcal{J}_\beta(M) = \mathcal{I}_{\beta-1}(M) - M^2 \mathcal{I}_\beta(M), \quad \text{(C2)}$$

$$\mathcal{K}_\beta(M) = \mathcal{I}_{\beta-2}(M) - 2M^2 \mathcal{I}_{\beta-1}(M) + M^4 \mathcal{I}_\beta(M), \quad \text{(C3)}$$

$$\mathcal{L}_\beta(M) = \mathcal{I}_{\beta-3}(M) - 3M^2 \mathcal{I}_{\beta-2}(M) + 3M^4 \mathcal{I}_{\beta-1}(M) - M^6 \mathcal{I}_\beta(M). \quad \text{(C4)}$$

At infinite volume these can be simplified using,

$$\mathcal{I}_\beta(M, L \to \infty) = \frac{1}{(4\pi)^{3/2}} \frac{\Gamma(\beta - \frac{3}{2})}{\Gamma(\beta)} \frac{1}{(M^2)^{\beta - 3/2}}, \quad \text{(C5)}$$

for $\beta > 3/2$.

In numerically evaluating these sums, it is useful to note that

$$\sum_{\vec{n}} \frac{1}{(|\vec{n}|^2 + x^2)^\beta} = \sum_{\vec{n}} \frac{E_{1-\beta}(|\vec{n}|^2 + x^2)}{\Gamma(\beta)} + \frac{\pi^{3/2}}{\Gamma(\beta)} \times \int_0^1 dt t^{\beta - 5/2} e^{-t x^2} \left[\sum_{\vec{n} \neq 0} e^{-\pi^2 |\vec{n}|^2 / t} + 1 \right] \quad \text{(C6)}$$

where $E_n(x)$ is the exponential integral function. This form is valid for $\beta > \frac{3}{2}$, $x \in \mathbb{R}$ and the remaining sums converge exponentially fast in $|\vec{n}|$.

[1] M. Schumacher, Prog. Part. Nucl. Phys. **55**, 567 (2005).
[2] C. E. Hyde-Wright and K. de Jager, Annu. Rev. Nucl. Part. Sci. **54**, 217 (2004).
[3] S. Ragusa, Phys. Rev. D **47**, 3757 (1993).
[4] B. R. Holstein, D. Drechsel, B. Pasquini, and M. Vanderhaeghen, Phys. Rev. C **61**, 034316 (2000).
[5] P. A. M. Guichon, G. Q. Liu, and A. W. Thomas, Nucl. Phys. **A591**, 606 (1995).
[6] H. R. Fiebig, W. Wilcox, and R. M. Woloshyn, Nucl. Phys. **B324**, 47 (1989).
[7] J. Christensen, W. Wilcox, F. X. Lee, and L. Zhou, Phys. Rev. D **72**, 034503 (2005).
[8] F. X. Lee, L. Zhou, W. Wilcox, and J. Christensen, Phys. Rev. D **73**, 034503 (2006).
[9] S. Weinberg, Phys. Rev. Lett. **17**, 616 (1966).
[10] J. Gasser and H. Leutwyler, Ann. Phys. (N.Y.) **158**, 142 (1984).
[11] J. Gasser and H. Leutwyler, Nucl. Phys. **B250**, 465 (1985).
[12] S. R. Sharpe and R. Singleton, Phys. Rev. D **58**, 074501 (1998).
[13] G. Rupak and N. Shoresh, Phys. Rev. D **66**, 054503 (2002).
[14] O. Bär, G. Rupak, and N. Shoresh, Phys. Rev. D **70**, 034508 (2004).

[15] S. R. Beane and M. J. Savage, Phys. Rev. D **68**, 114502 (2003).
[16] S. Rai Choudhury and D. Z. Freedman, Phys. Rev. **168**, 1739 (1968).
[17] M. Gell-Mann and M. L. Goldberger, Phys. Rev. **96**, 1433 (1954).
[18] F. E. Low, Phys. Rev. **96**, 1428 (1954).
[19] F. Fucito, G. Parisi, and S. Petrarca, Phys. Lett. B **115**, 148 (1982).
[20] G. Martinelli, G. Parisi, R. Petronzio, and F. Rapuano, Phys. Lett. B **116**, 434 (1982).
[21] C. W. Bernard, T. Draper, K. Olynyk, and M. Rushton, Phys. Rev. Lett. **49**, 1076 (1982).
[22] S. Aoki and A. Gocksch, Phys. Rev. Lett. **63**, 1125 (1989).
[23] S. Aoki, A. Gocksch, A. V. Manohar, and S. R. Sharpe, Phys. Rev. Lett. **65**, 1092 (1990).
[24] E. Shintani *et al.*, PoS, LAT2005 (2005) 128.
[25] J. M. Zanotti *et al.* (private communication).
[26] W. Detmold, Phys. Rev. D **71**, 054506 (2005).
[27] D. Babusci, G. Giordano, A. I. L'vov, G. Matone, and A. M. Nathan, Phys. Rev. C **58**, 1013 (1998).
[28] J. S. Schwinger, Phys. Rev. **82**, 664 (1951).
[29] E. Jenkins and A. V. Manohar, Phys. Lett. B **255**, 558 (1991).
[30] E. Jenkins and A. V. Manohar, Workshop on Effective Field Theories of the Standard Model, Dobogoko, Hungary, 1991 (1991).
[31] E. Jenkins and A. V. Manohar, Phys. Lett. B **259**, 353 (1991).
[32] V. Bernard, N. Kaiser, and U.-G. Meißner, Z. Phys. C **60**, 111 (1993).
[33] D. Arndt and B. C. Tiburzi, Phys. Rev. D **69**, 014501 (2004).
[34] B. C. Tiburzi, Phys. Rev. D **72**, 094501 (2005).
[35] J. N. Labrenz and S. R. Sharpe, Phys. Rev. D **54**, 4595 (1996).
[36] M. J. Savage, Nucl. Phys. **A700**, 359 (2002).
[37] J.-W. Chen and M. J. Savage, Phys. Rev. D **65**, 094001 (2002).
[38] S. R. Beane and M. J. Savage, Nucl. Phys. **A709**, 319 (2002).
[39] S. R. Sharpe and N. Shoresh, Int. J. Mod. Phys. A **16**, 1219 (2001).
[40] B. C. Tiburzi, Phys. Rev. D **71**, 054504 (2005).
[41] W. Detmold and C. J. D. Lin, Phys. Rev. D **71**, 054510 (2005).
[42] J. Wess and B. Zumino, Phys. Lett. B **37**, 95 (1971).
[43] E. Witten, Nucl. Phys. **B223**, 422 (1983).
[44] D. Arndt and B. C. Tiburzi, Phys. Rev. D **68**, 114503 (2003).
[45] M. E. Luke and A. V. Manohar, Phys. Lett. B **286**, 348 (1992).
[46] B. C. Tiburzi and A. Walker-Loud, Nucl. Phys. **A764**, 274 (2006).
[47] N. Fettes, U.-G. Meißner, M. Mojzis, and S. Steininger, Ann. Phys. (N.Y.) **283**, 273 (2000).
[48] M. N. Butler, M. J. Savage, and R. P. Springer, Nucl. Phys. **B399**, 69 (1993).
[49] B. C. Tiburzi, Phys. Rev. D **71**, 034501 (2005).
[50] J. S. Bell and R. Jackiw, Nuovo Cimento A **60**, 47 (1969).
[51] S. L. Adler, Phys. Rev. **177**, 2426 (1969).
[52] S. L. Adler and W. A. Bardeen, Phys. Rev. **182**, 1517 (1969).
[53] J. Bijnens, L. Girlanda, and P. Talavera, Eur. Phys. J. C **23**, 539 (2002).
[54] S. R. Sharpe and R. S. Van de Water, Phys. Rev. D **69**, 054027 (2004).
[55] V. Bernard, N. Kaiser, and U.-G. Meißner, Phys. Rev. Lett. **67**, 1515 (1991).
[56] V. Bernard, N. Kaiser, and U.-G. Meißner, Nucl. Phys. **B373**, 346 (1992).
[57] M. N. Butler and M. J. Savage, Phys. Lett. B **294**, 369 (1992).
[58] T. R. Hemmert, B. R. Holstein, and J. Kambor, Phys. Rev. D **55**, 5598 (1997).
[59] T. R. Hemmert, B. R. Holstein, J. Kambor, and G. Knöchlein, Phys. Rev. D **57**, 5746 (1998).
[60] V. Pascalutsa and D. R. Phillips, Phys. Rev. C **67**, 055202 (2003).
[61] V. Pascalutsa and D. R. Phillips, Phys. Rev. C **68**, 055205 (2003).
[62] V. Bernard, N. Kaiser, U.-G. Meißner, and A. Schmidt, Z. Phys. A **348**, 317 (1994).
[63] V. Bernard, N. Kaiser, A. Schmidt, and U.-G. Meißner, Phys. Lett. B **319**, 269 (1993).
[64] X.-D. Ji, C.-W. Kao, and J. Osborne, Phys. Rev. D **61**, 074003 (2000).
[65] K. B. Vijaya Kumar, J. A. McGovern, and M. C. Birse, Phys. Lett. B **479**, 167 (2000).
[66] G. C. Gellas, T. R. Hemmert, and U.-G. Meißner, Phys. Rev. Lett. **85**, 14 (2000).
[67] J. A. McGovern, Phys. Rev. C **63**, 064608 (2001).
[68] S. R. Beane, M. Malheiro, J. A. McGovern, D. R. Phillips, and U. van Kolck, Phys. Lett. B **567**, 200 (2003).
[69] S. R. Beane, M. Malheiro, J. A. McGovern, D. R. Phillips, and U. van Kolck, Nucl. Phys. **A747**, 311 (2005).
[70] D. Arndt and B. C. Tiburzi, Phys. Rev. D **68**, 094501 (2003).
[71] P. F. Bedaque and M. J. Savage, Phys. Rev. C **62**, 018501 (2000).
[72] W. Detmold and M. J. Savage, Nucl. Phys. **A743**, 170 (2004).
[73] J.-W. Chen, Phys. Lett. B **543**, 183 (2002).
[74] J. Gasser and H. Leutwyler, Phys. Lett. B **188**, 477 (1987).
[75] W. Detmold and M. J. Savage, Phys. Lett. B **599**, 32 (2004).
[76] S. R. Sharpe, Phys. Rev. D **46**, 3146 (1992).